New Journal Chemistry

Structural and Bio-Catalytic Aspects of Nano Crystallite Iron(III) Complexes Containing Triazole-Based Ligands

Ali M. A. Al-Nashawy[a], Abd El-Motaleb M. Ramadan[a]*, Shaban Y. Shaban[a], Said Khalil[b], Magdy Shebl[b], Mohamed M. Abdel-Galeil[c], Sami A. Al-Harbie[d], Ahmed M. Fathy[e]

[a]Chemistry Department, Faculty of Science, Kafr El-Sheikh University, Kafr El-Sheikh, Egypt
[b]Chemistry Department, Faculty of Education, Ain Shams University, Roxy, Cairo, Egypt
[c]Analytical and Electrochemistry Research Unit, Chemistry Department, Faculty of Science, Tanta University, Gharbia, 31527- Tanta, Egypt.
[d]Chemistry Department, University College in Al-Jamoum, Umm Al-Qura University, Makkah, Saudi Arabia
[e]Chemistry Department, Faculty of Science, Zagazig University, Zagazig, Egypt

Supplementary Information

S1: Experimental

S1.1. Materials

All chemicals used were of analytical grade. The benzoyl hydrazine, hydrazine hydrate 95%, 2,5-dibromo methylbenzene and 2,6-dibromo methyl pyridine were purchased from Aldrich. 2,3-Dibromo methyl quinoxaline was synthesized based on the method reported in literature [28-30]. Phenyl triazole was prepared according to the modified method described below.

S1.2. *Preparation of phenyl triazole*

CS_2 (0.15 mole) was added drop wise to an ice cold solution of KOH (9.12 gm, 0.16 mol) in absolute ethanol (200 ml) containing benzoyl hydrazine (0.1 mol). The reaction mixture was diluted with ethanol (150 ml) and stirred for 2h at room temperature. Dry ether (200 ml) was added and the resulting solid K-salt precipitate was collected, washed with ether and finally dried.

A solution of the latter K-salt (0.05 mol) and hydrazine hydrate 95 % (0.5 mol) was heated under reflux with stirring for one hour. 5 ml of water was then added and the reaction mixture was neutralized with concentrated hydrochloric acid. The solid obtained

upon neutralization was collected and crystallized from acetic acid to give colorless crystals of phenyl-triazole (mp. 214-216 °C).

S1.3. Preparation of the pyridine based ligand (L^1, L^2 and L^3)

To a solution of phenyl triazole (50 mmol) in aqueous ethanol (50 ml) containing KOH (50 mmol) the appropriate dibromo compound (25 mmol) was added. The reaction mixture was heated under reflux for 1 h. The solvent was then removed in vacuum and the remaining solid was collected and crystallized from DMF to give colorless crystals of the triazole – based ligands L^1, L^2 and L^3.

S1.4. *Physical measurements*

IR spectra were recorded using KBr disks in the 4000-200 cm^{-1} range on a Unicam SP200 spectrophotometer. The electronic absorption spectra were obtained in DMF solution with a Shimadzu UV-240 spectrophotometer. Magnetic moments were measured by Gouy's method at room temperature. ESR measurements of the polycrystalline samples at room temperature were made on a Varian E9 X-band spectrometer using a quartz Dewar vessel. All spectra were calibrated with DPPH (g = 2.0027). The specific conductance of the complexes was measured using freshly prepared 10^{-3} M solutions in electrochemically pure DMF at room temperature, using an YSI Model 32 conductance meter. The thermogravimetric measurements were performed using a Shimadzu TG 50-Thermogravimetric analyzer in the 25-1000 °C range and under an N_2 atmosphere. Elemental analyses (C, H, and N) were carried out at the Micro analytical Unit of Cairo University.

S1.5. Cyclic voltammetry measurements

The cyclic voltammetry measurements were carried out in the potential range of -500 to 1000 mV at different scan rates ranging from 10 to 100 mV/s. The concentration of the metal complex in a methanol solution 0.2 mM and (n-butyl) ammonium perchlorate (0.001M) was the supporting electrolyte. Electrochemical impedance spectroscopy (EIS) measurements were performed with an open circuit potential and over a frequency range from 100 kHz to 10 mHz.

Electrochemical Analyzers Models 263A and 273-PAR with a computer-controlled using software package 270/250-PAR (Princeton Applied Research, Oak Ridge, TN,

USA) were used for the voltammetric measurements. A voltammetric cell consist of a glassy carbon-working electrode (5mm), an Ag/AgCl/KCls reference electrode (BASi-MF-2079), and a platinum wire counter electrode (BASi-MW-1032) was used in the present investigation.

S1.6. Oxidase biomimetic catalytic activity

A mixture of 1.0 ml of studied substrate 3,5-DTBCH_2 or *o*-APH_3 solution (50 mM) in methanol and 1.0 ml of copper complex solution (0.5 mM) in DMF was placed in a 1 cm path length optical cell containing 1.0 ml of methanol in a spectrophotometer. The final concentration of reaction mixture is catechol or *o*-aminophenol (10 mM) and complex (l mM). The formation of 3,5-di-*tert*-butyl-quinone (3,5-DTBQ) was followed by observing the increase of characteristic quinone absorption band at 400 nm and for 2-amino-3*H*-phenoxazine-3-one (APX) at 433 nm. Kinetic studies were performed on a *Kinet Asyst SF*-61DX2 stopped–flow instrument (thermostatted at 23 °C) with an optical path length of 1 cm, at 400 nm for 3,5–di-*tert*-butyl catechol and 433 nm for ortho--aminophenol.

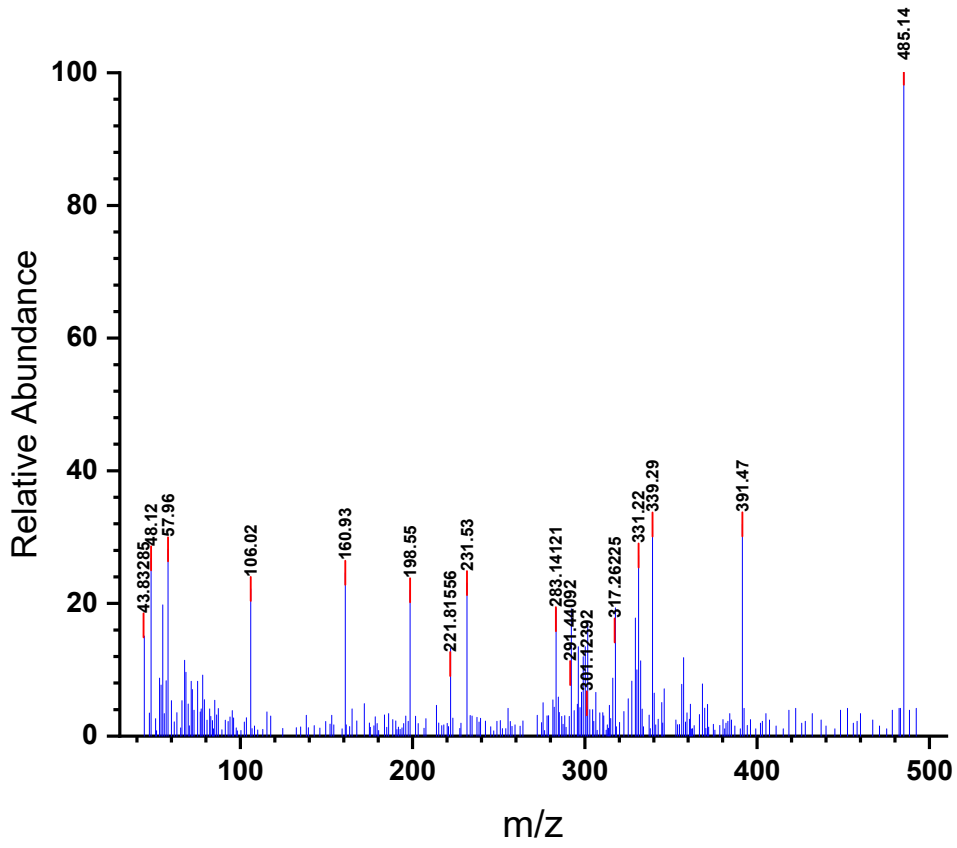

S2: EI-MS spectrum pattern of the triazole – based ligand L^1

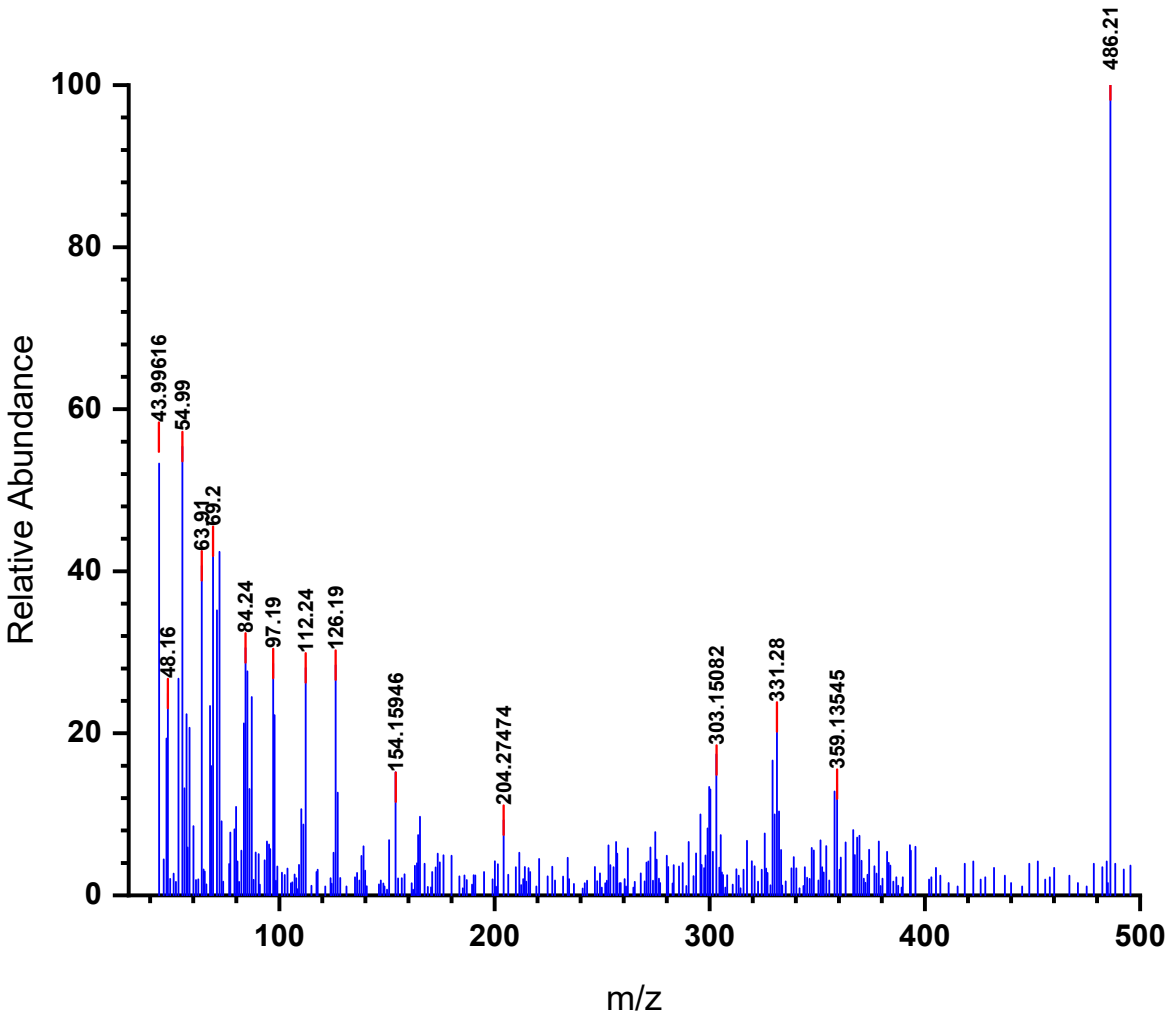

S3: EI-MS spectrum pattern of the triazole – based ligand $\mathbf{L^2}$

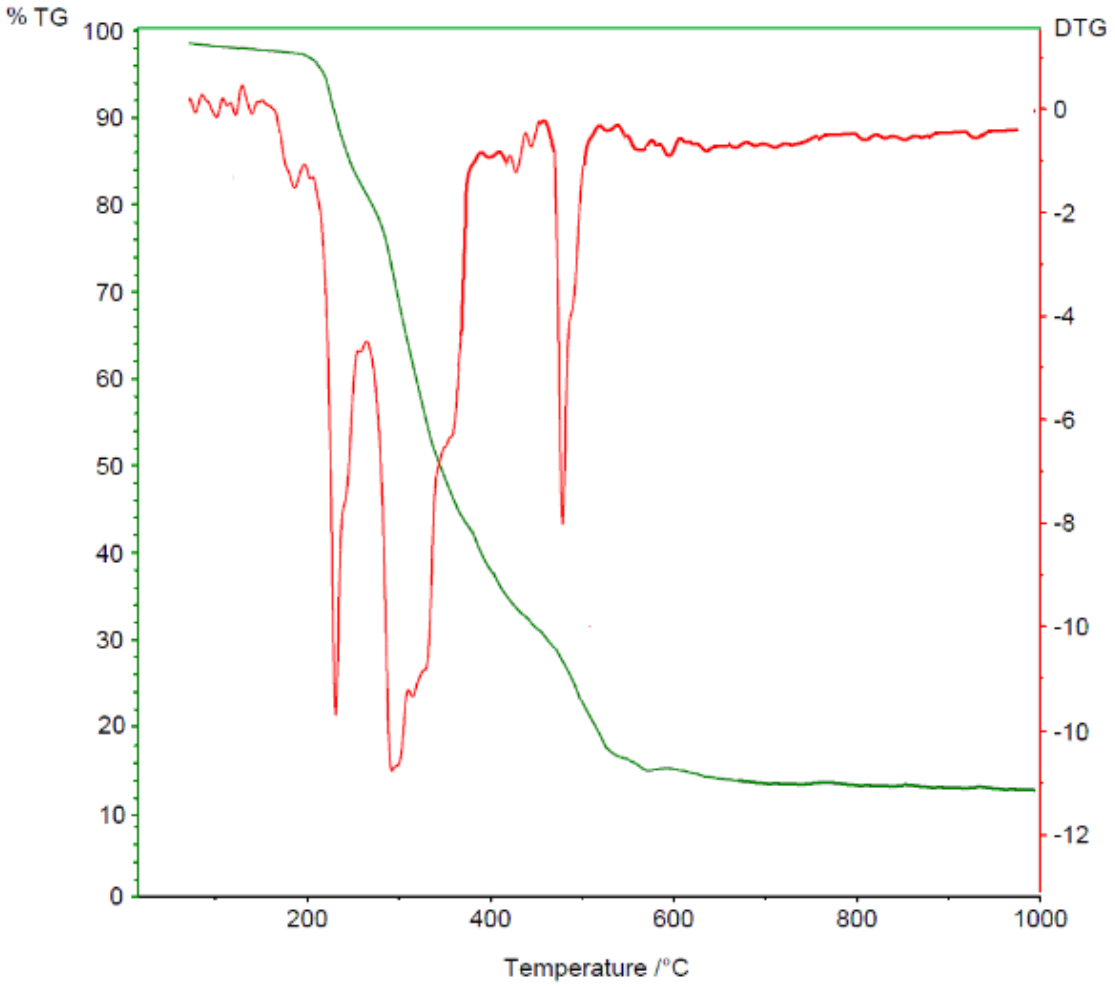

S4: TGA and DTG plots of complex 1

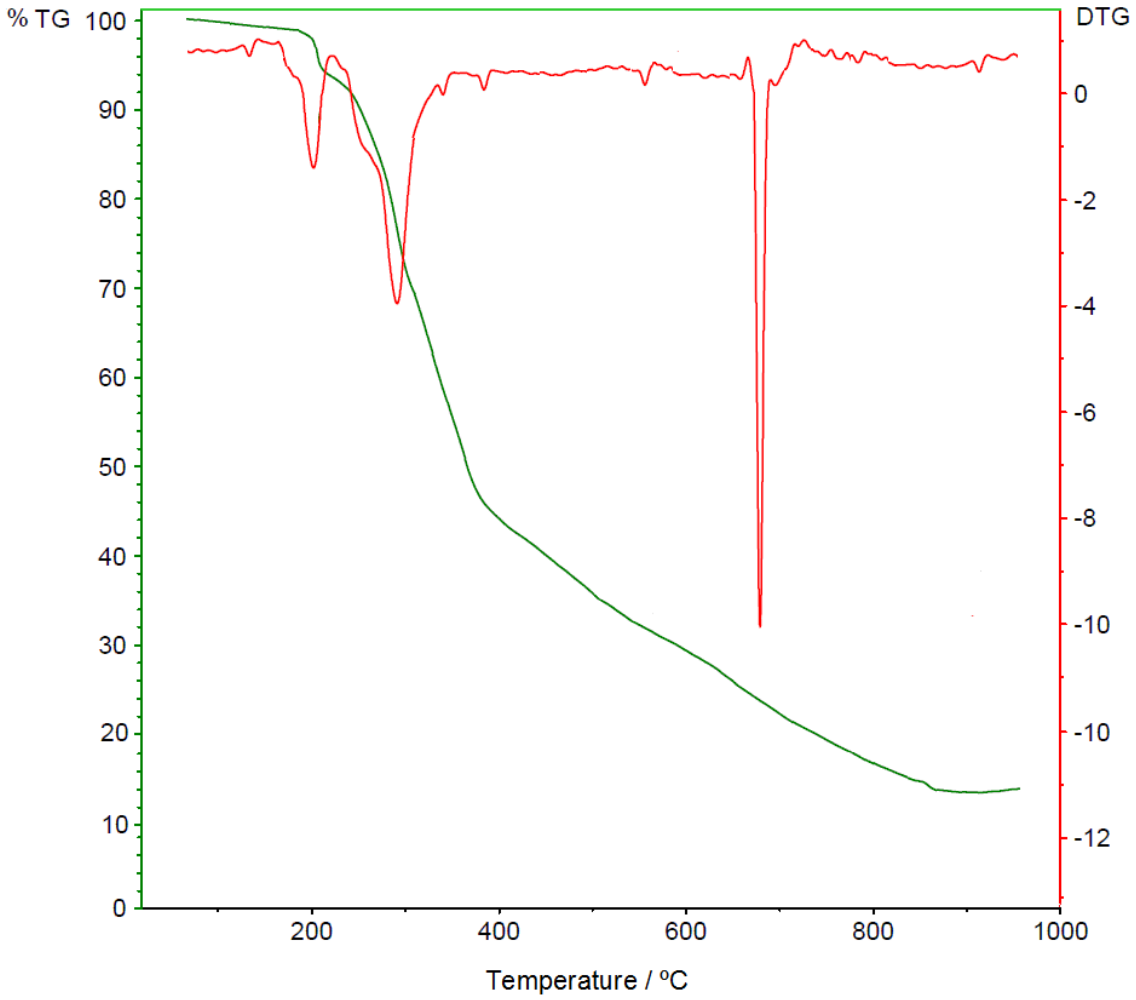

S5: TGA and DTG plots of complex 2

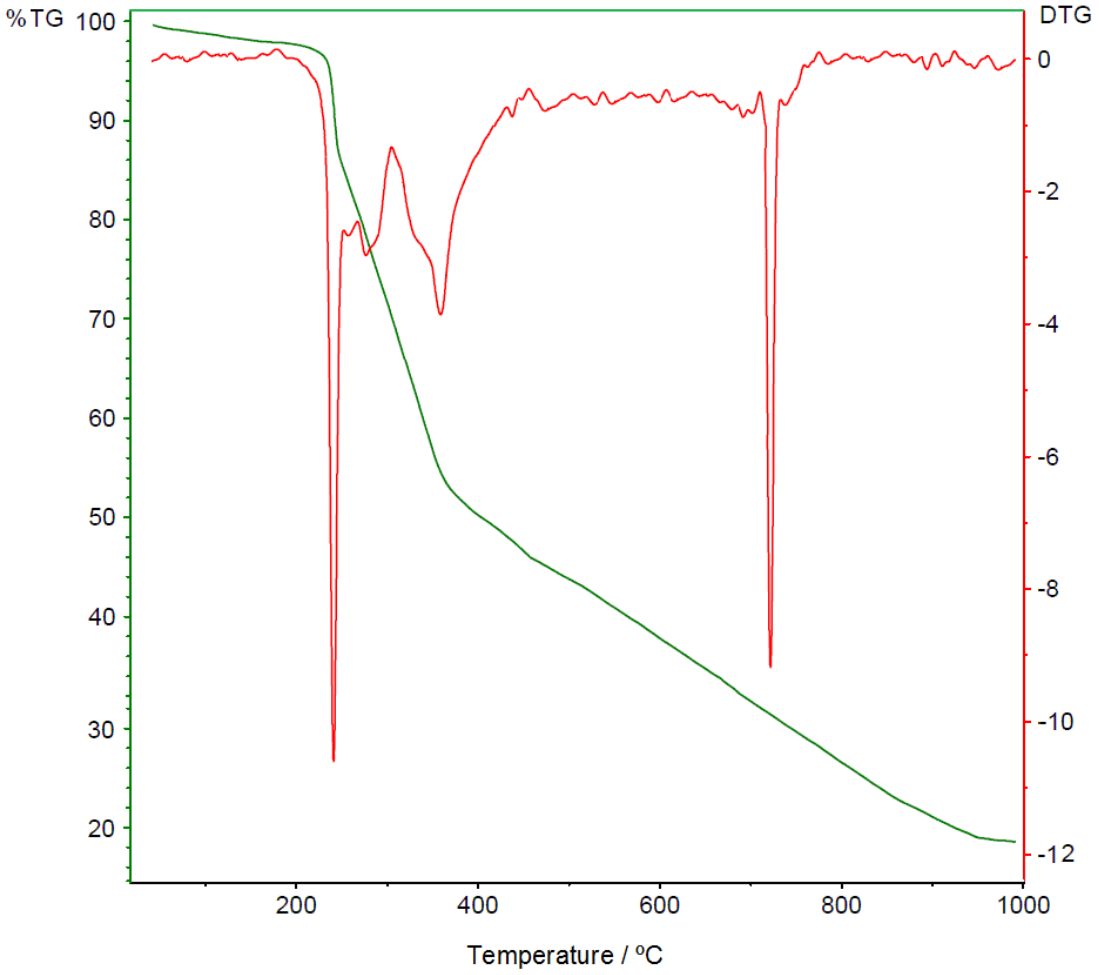

S6: TGA and DTG plots of complex 3

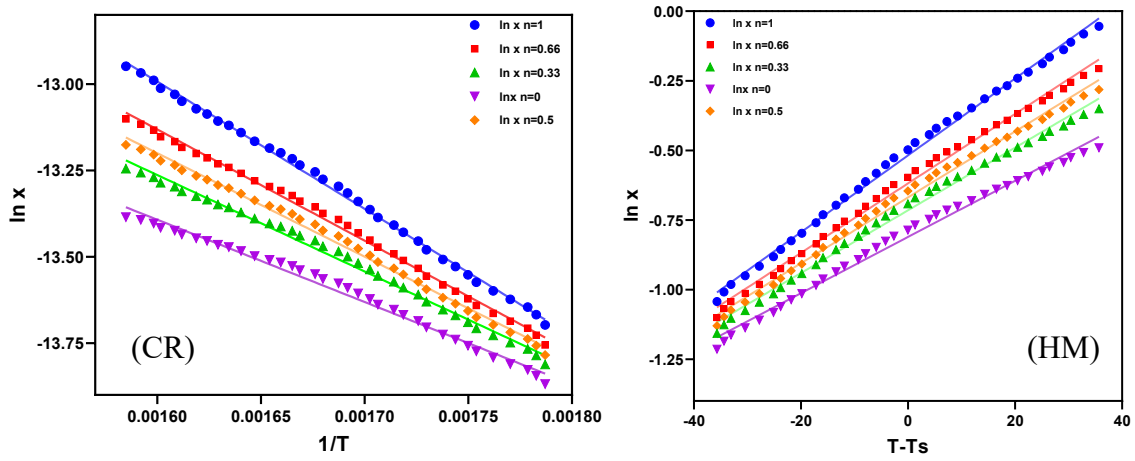

1st step

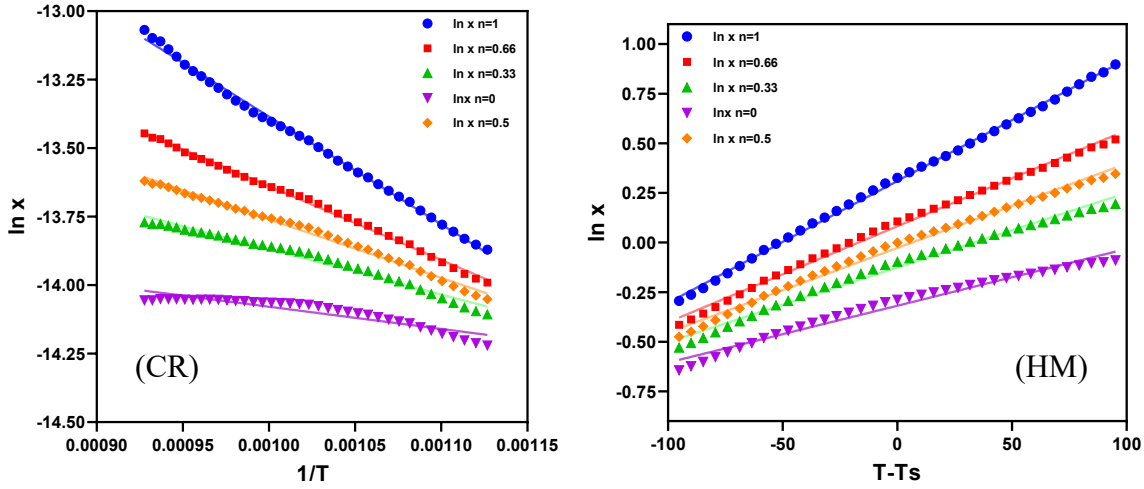

2nd step

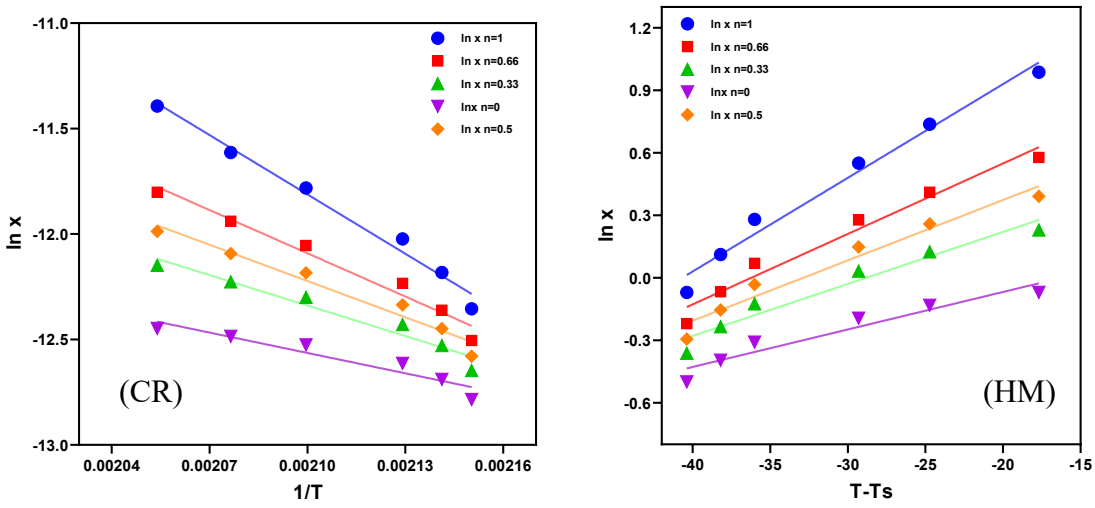

3rd step

S7: Coats–Redfern (CR) and Horowitz-Metzger (HM) plots of the pyrolysis steps of complex **2**

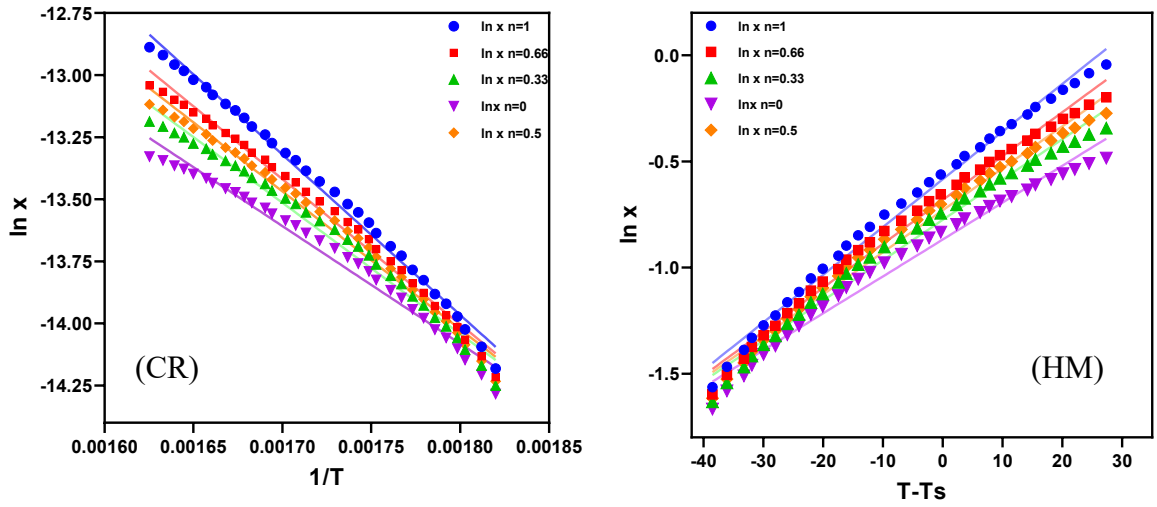

1st step

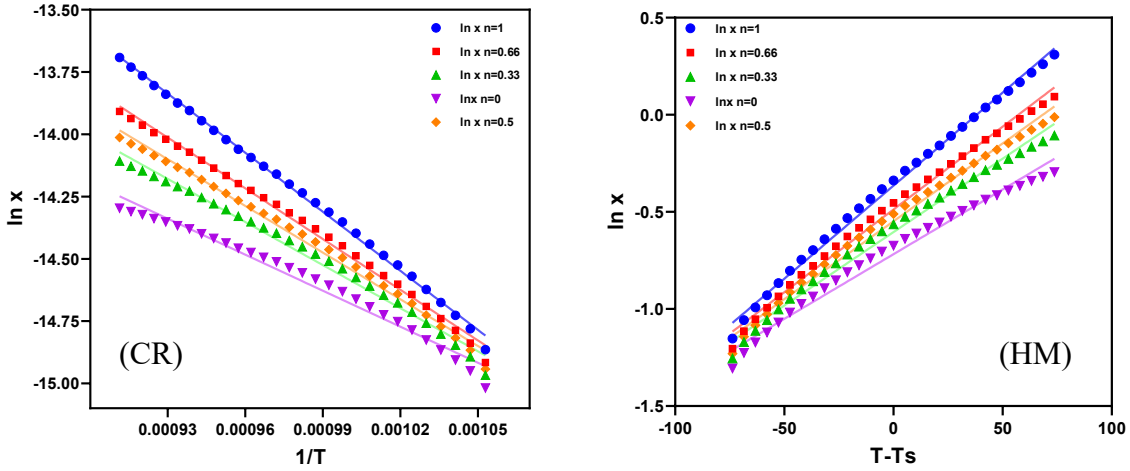

2nd step

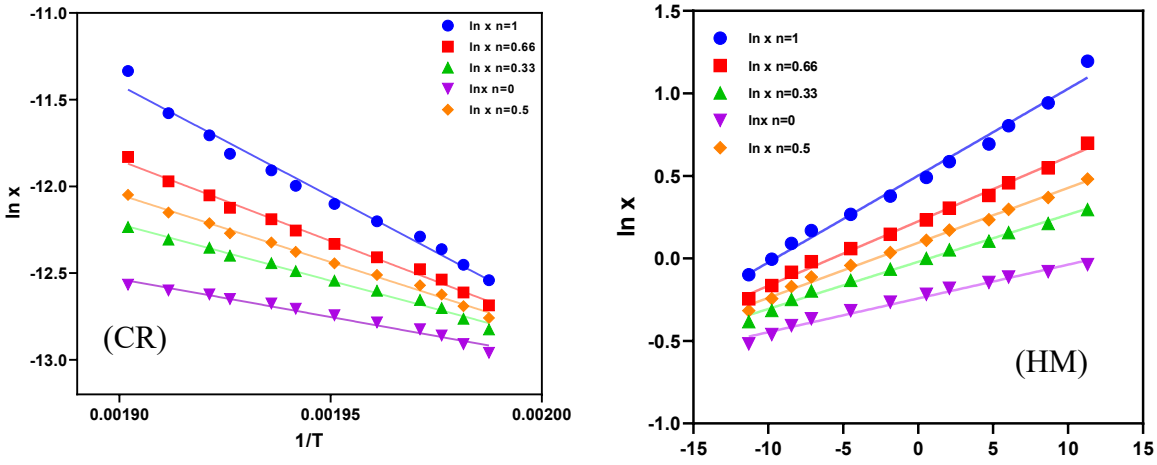

3rd step

S8: Coats–Redfern (CR) and Horowitz-Metzger (HM) plots of the pyrolysis steps of complex **3**

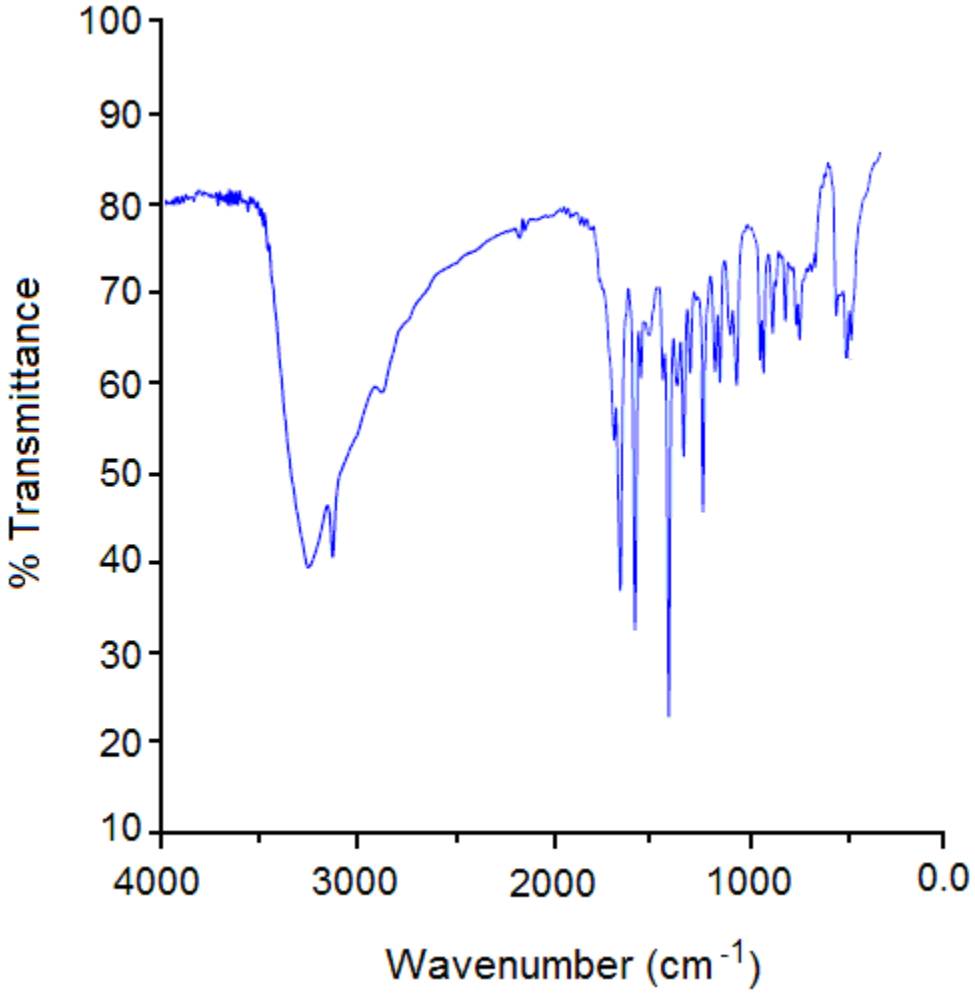

S9: FTIR spectrum of the triazole – based ligand (L^1)

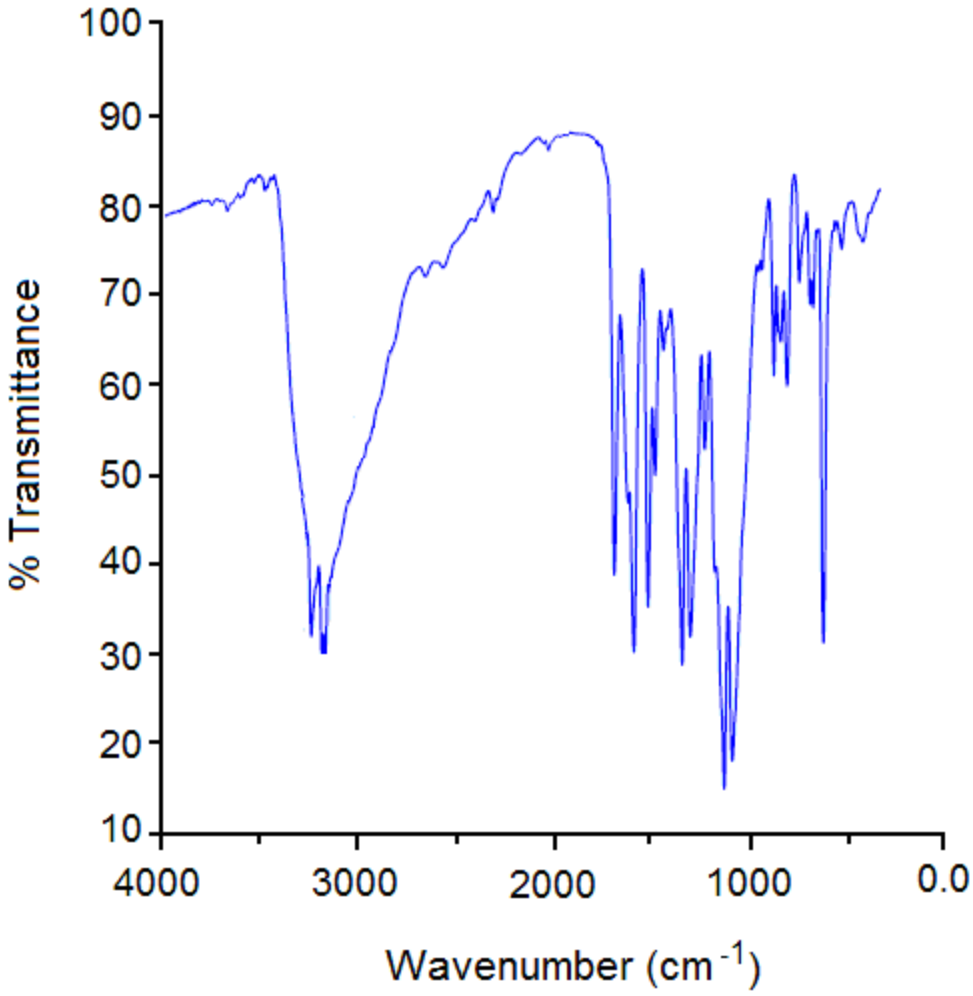

S10. FTIR spectrum of the triazole – based iron(III) complex 1

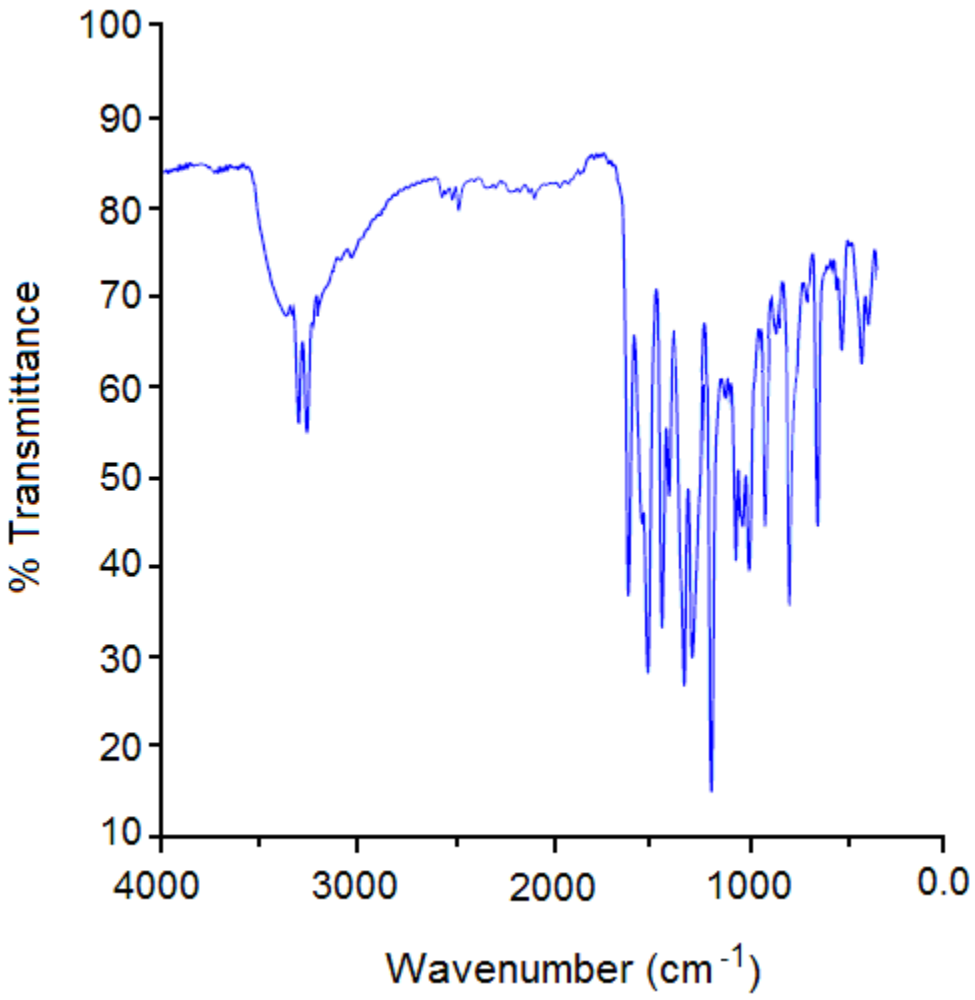

S11: FTIR spectrum of the triazole – based ligand (L^2)

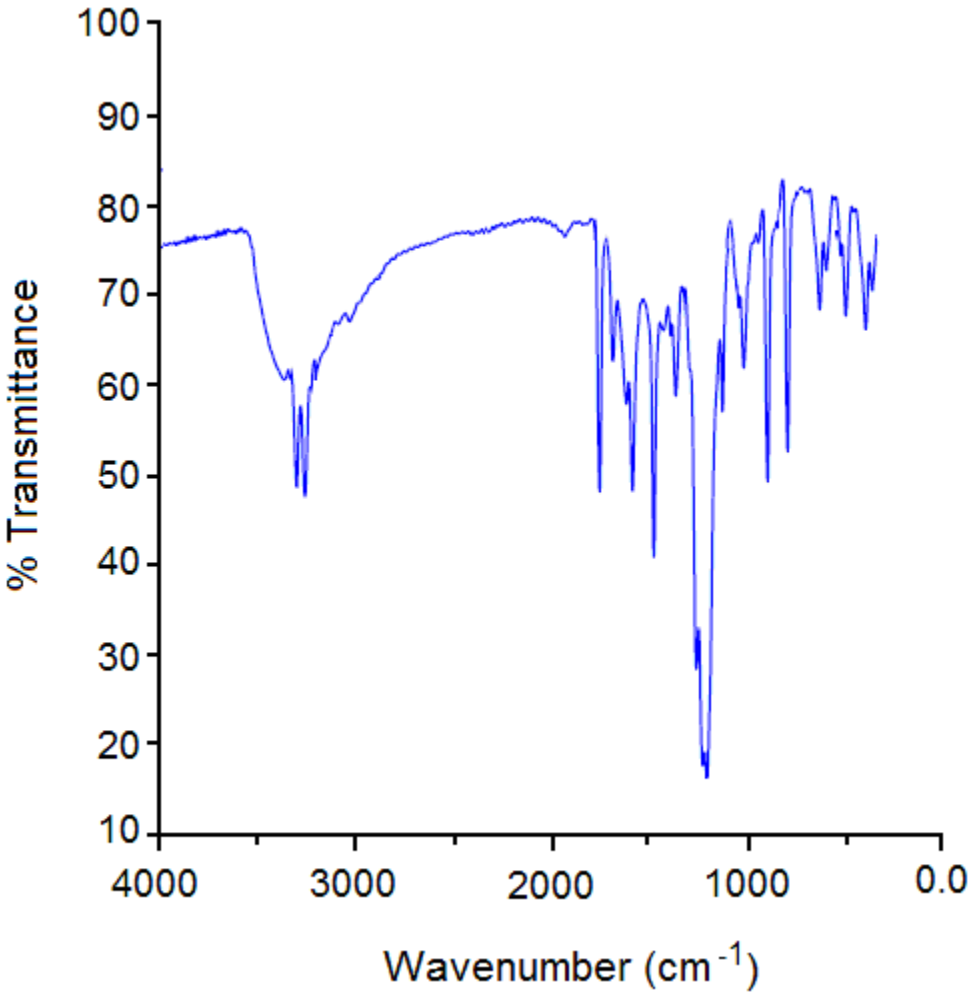

S12. FTIR spectrum of the triazole – based iron(III) complex 2

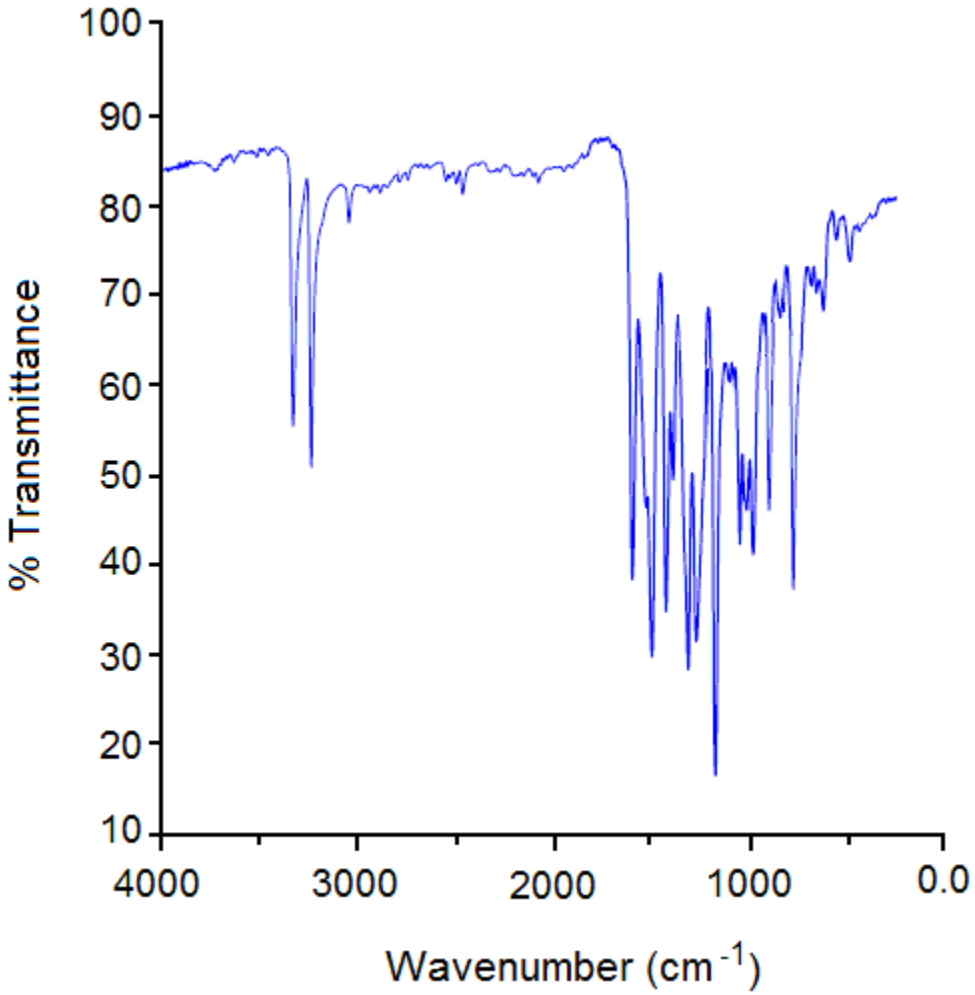

S13: FTIR spectrum of the triazole – based ligand L^3

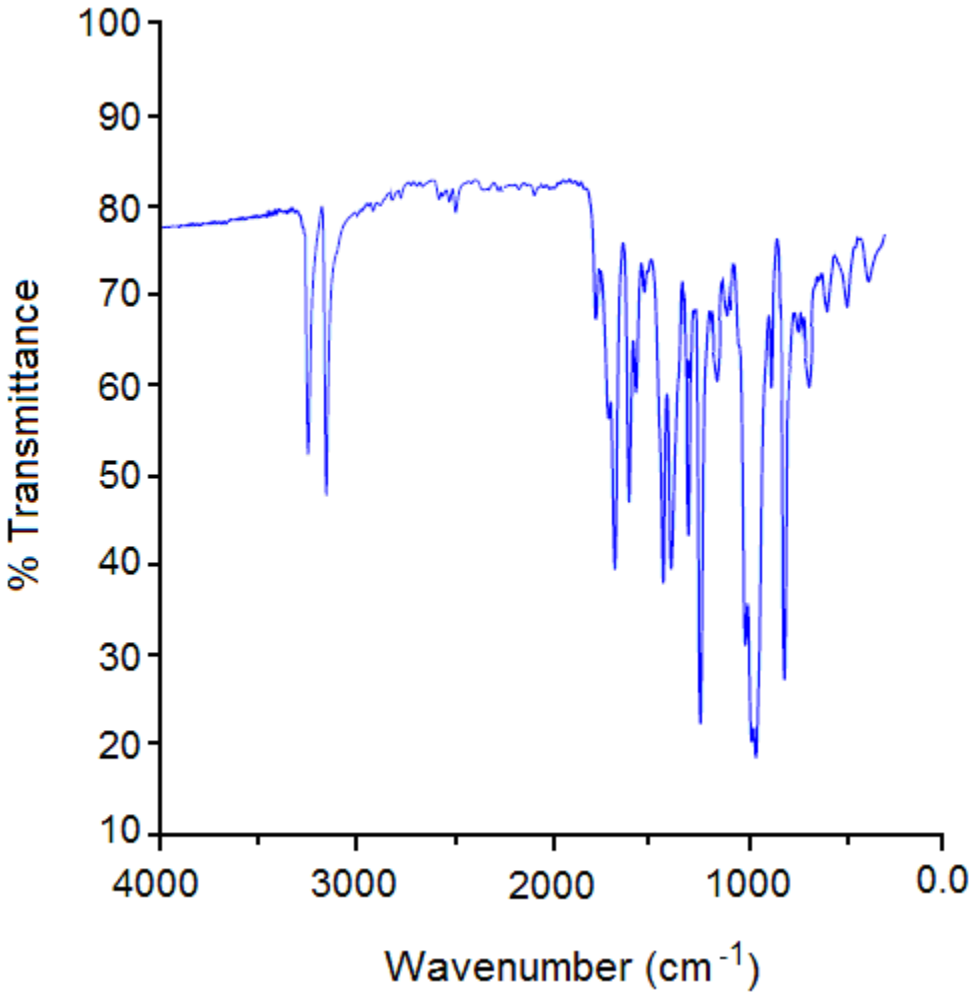

S14: FTIR spectrum of the triazole – based iron(III) complex 3

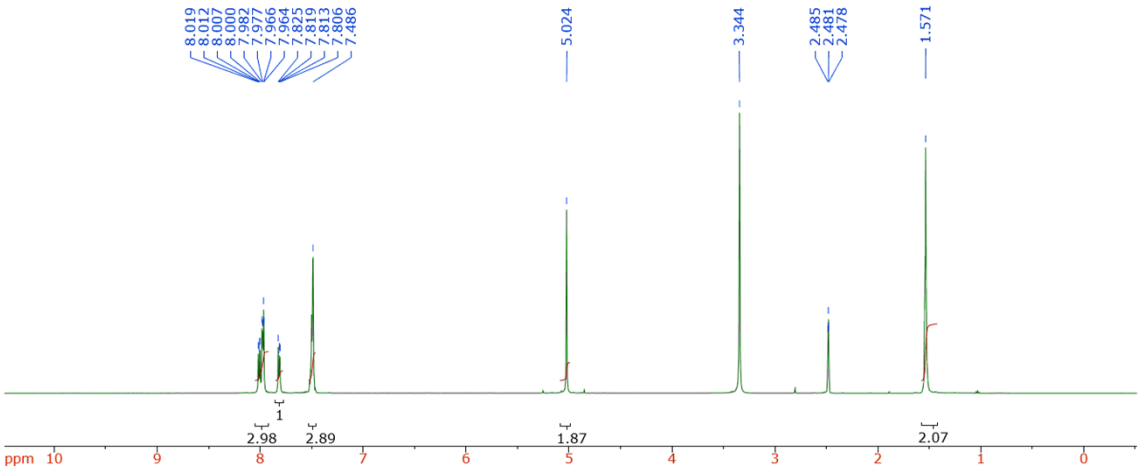

S15: Proton NMR spectrum of the free organic ligand L^1

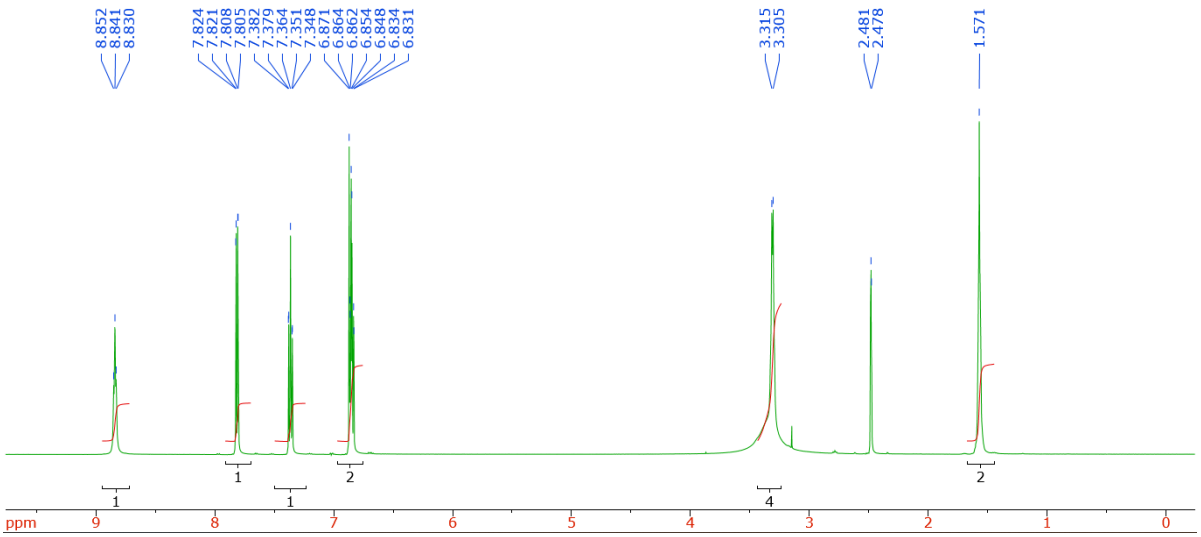

S16: Proton NMR spectrum of the free organic ligand L^2

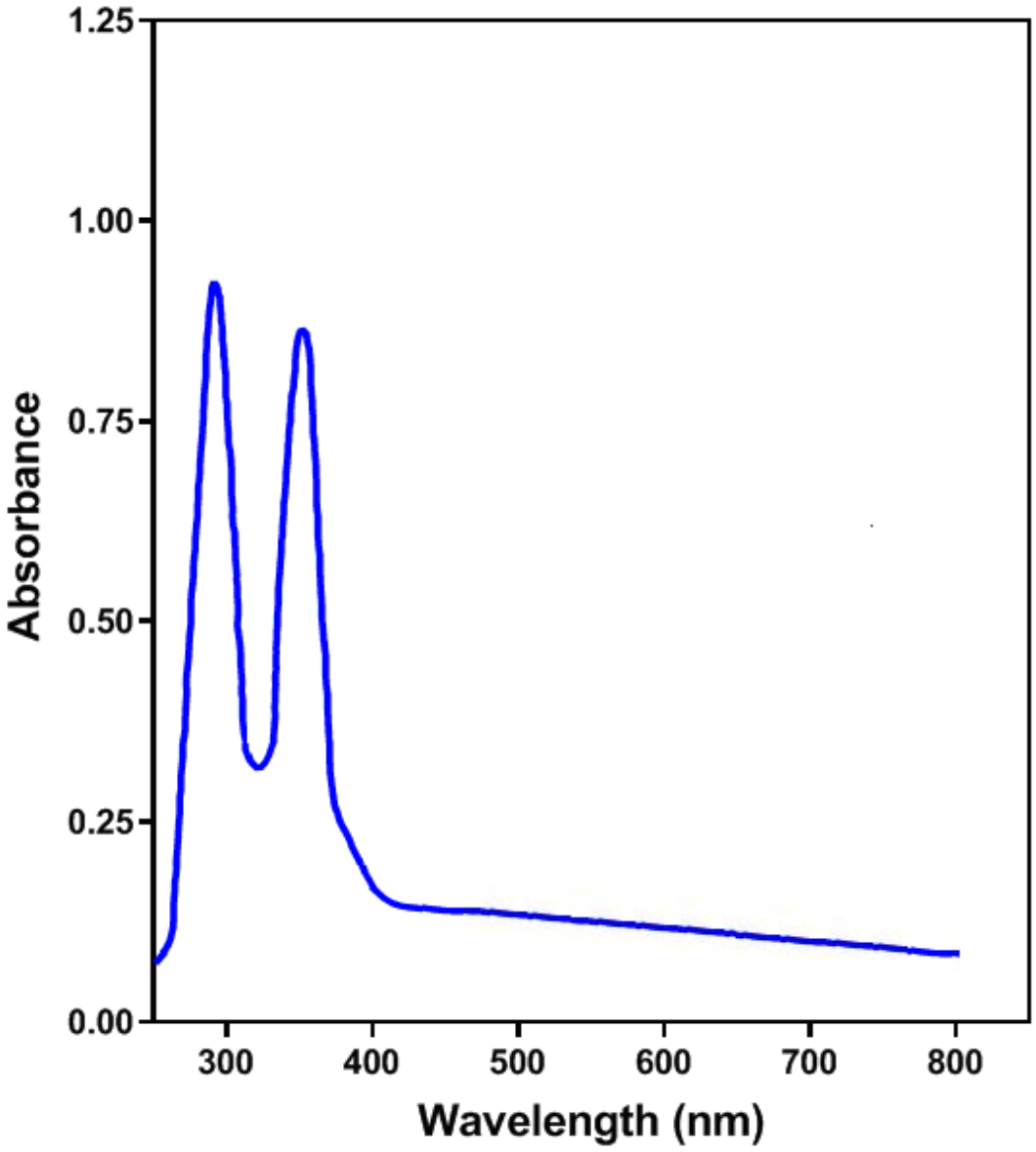

S17: Electronic absorption spectrum of L^1

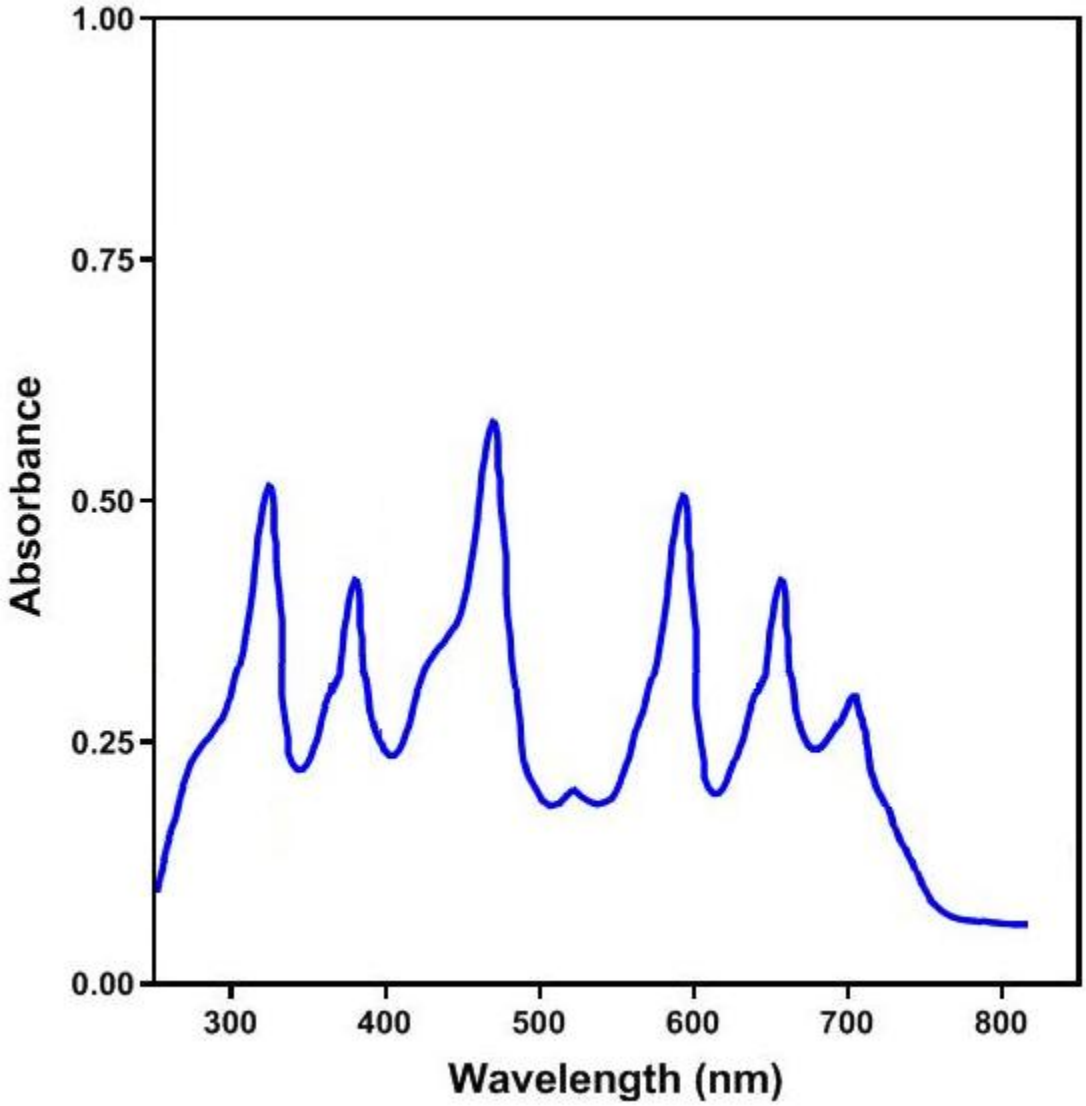

S18: Electronic absorption spectrum of triazole – based iron(III) complex 1

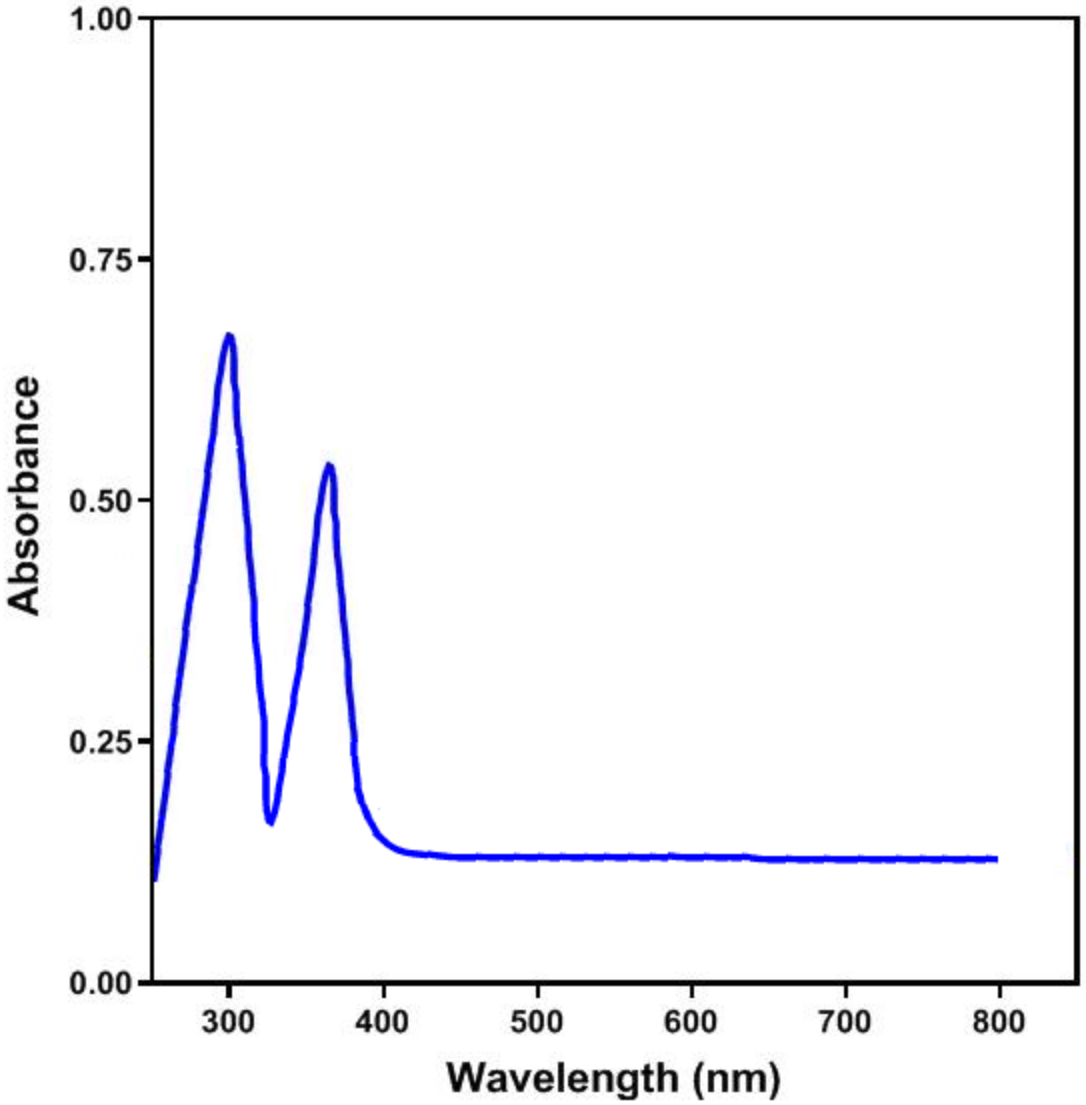

S19: Electronic absorption spectrum of L^2

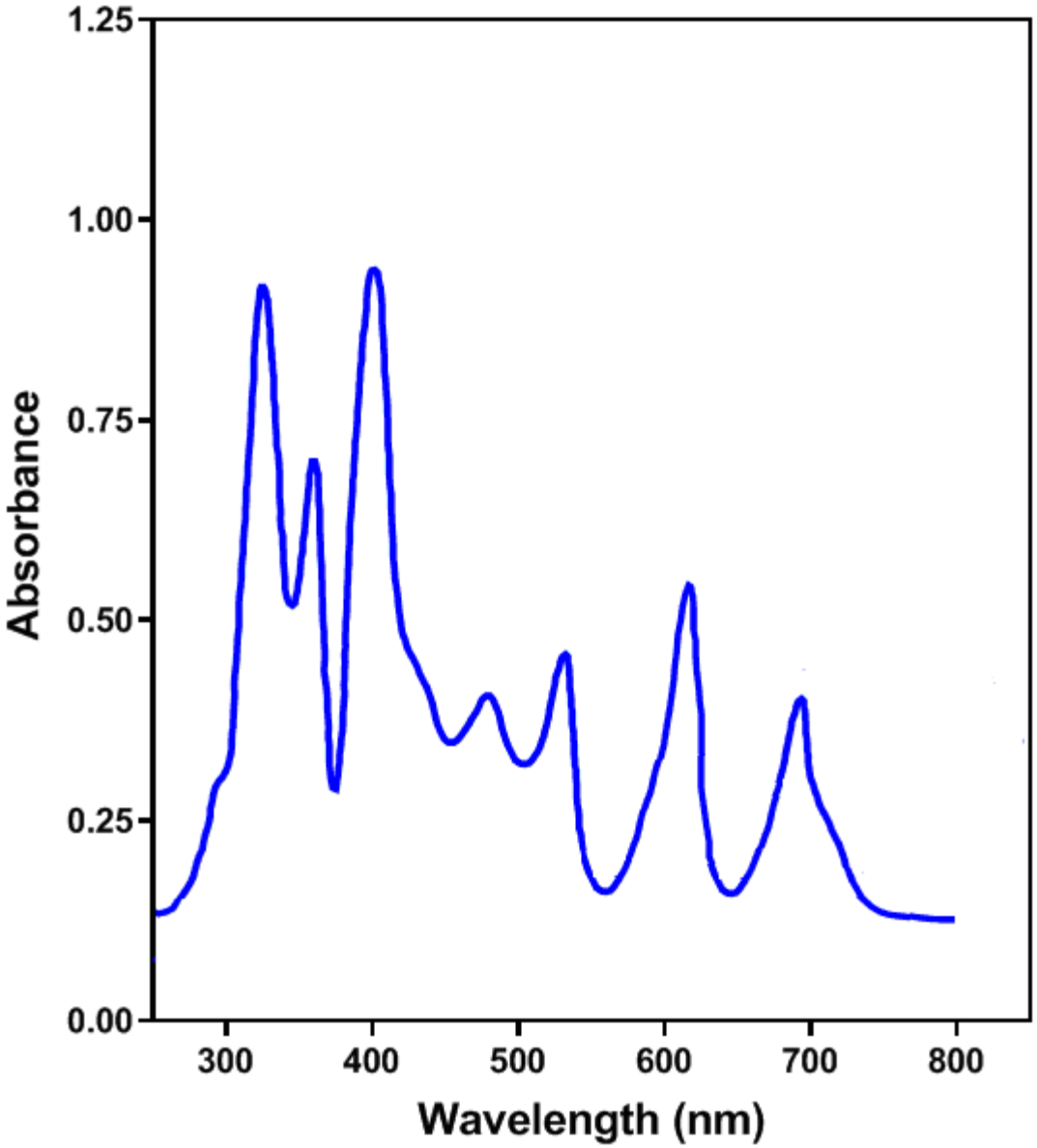

S20: Electronic absorption spectrum of triazole – based iron(III) complex 2

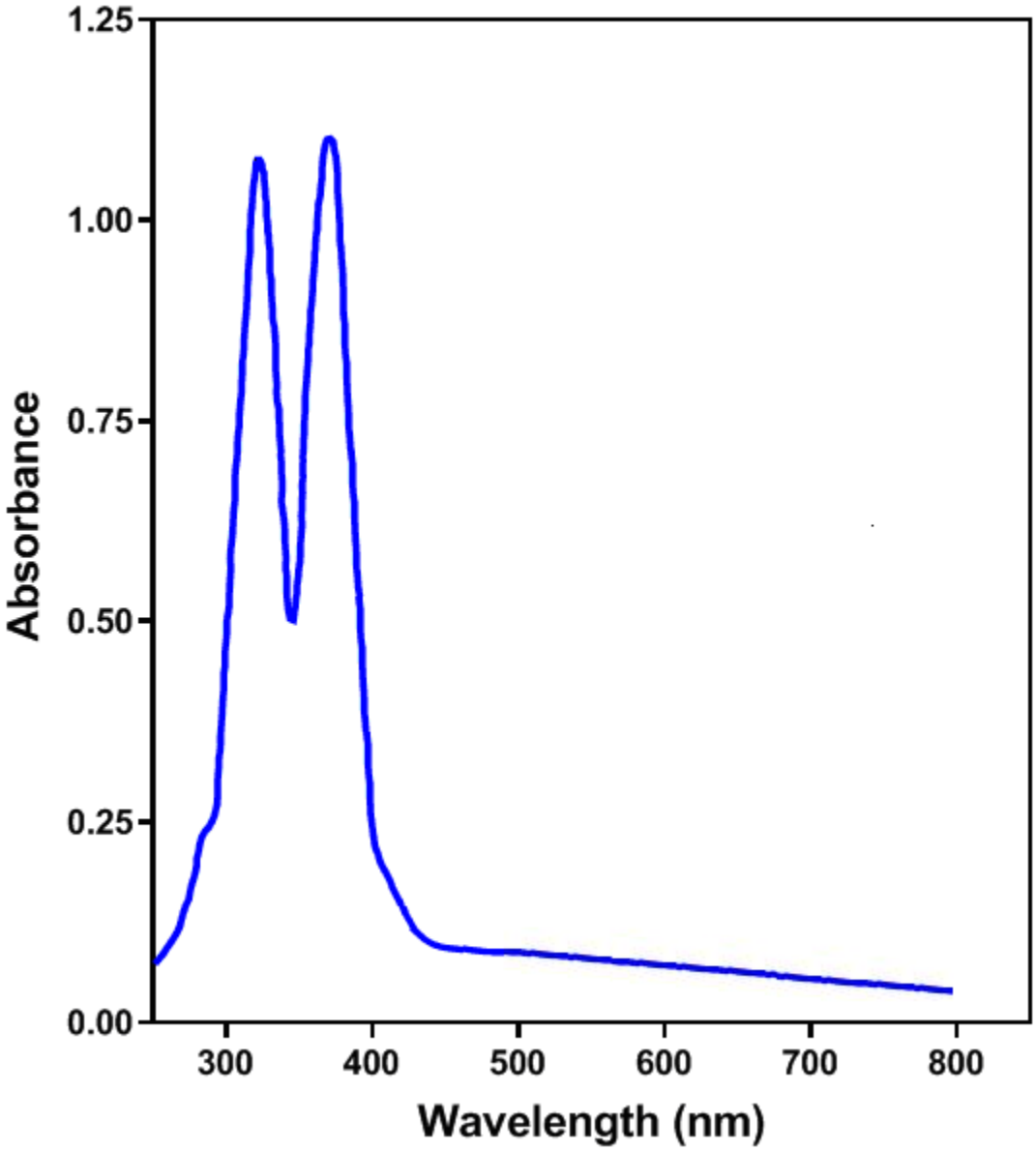

S21: Electronic absorption spectrum of L^3

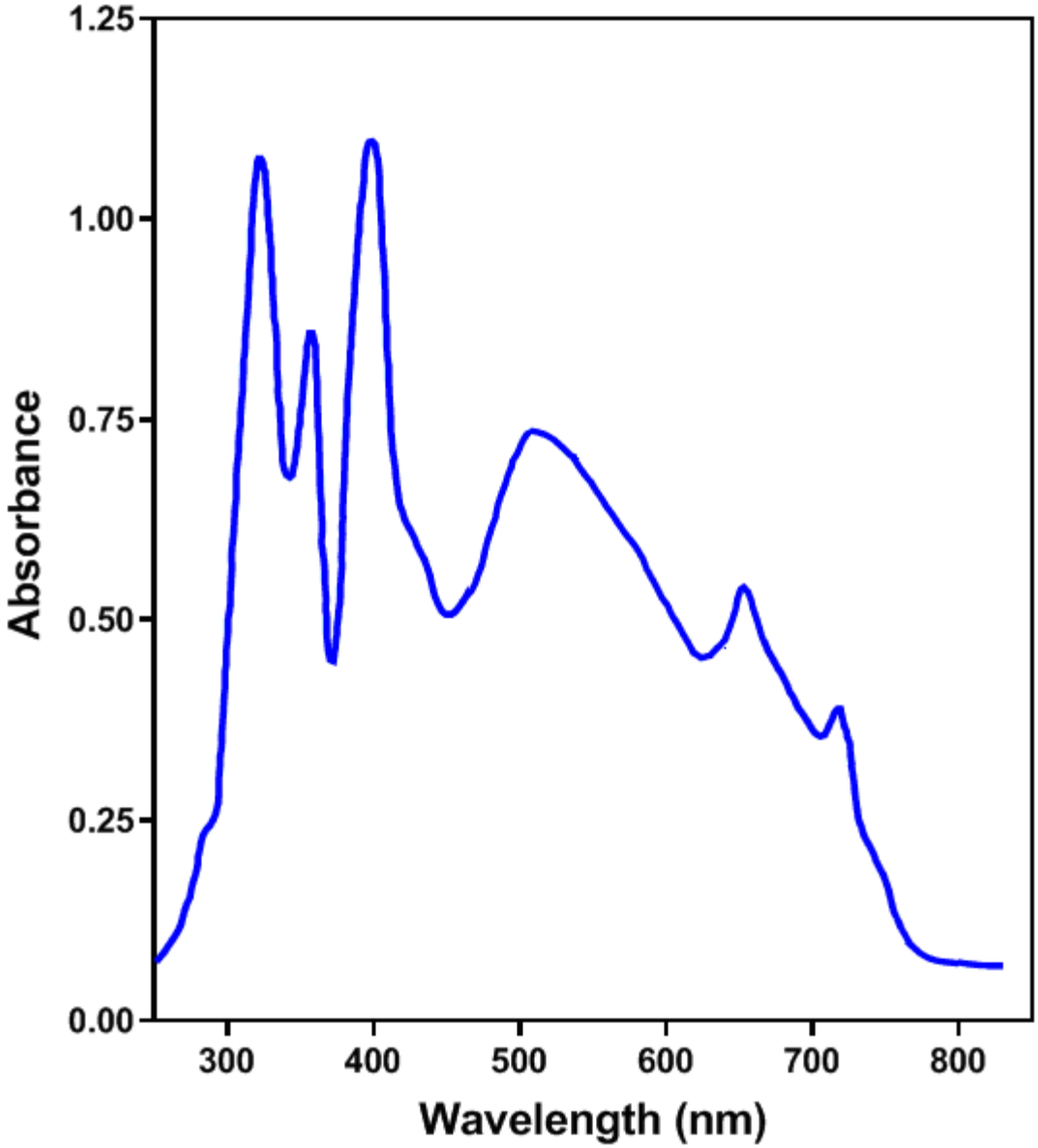

S22: Electronic absorption spectrum of triazole – based iron(III) complex 3

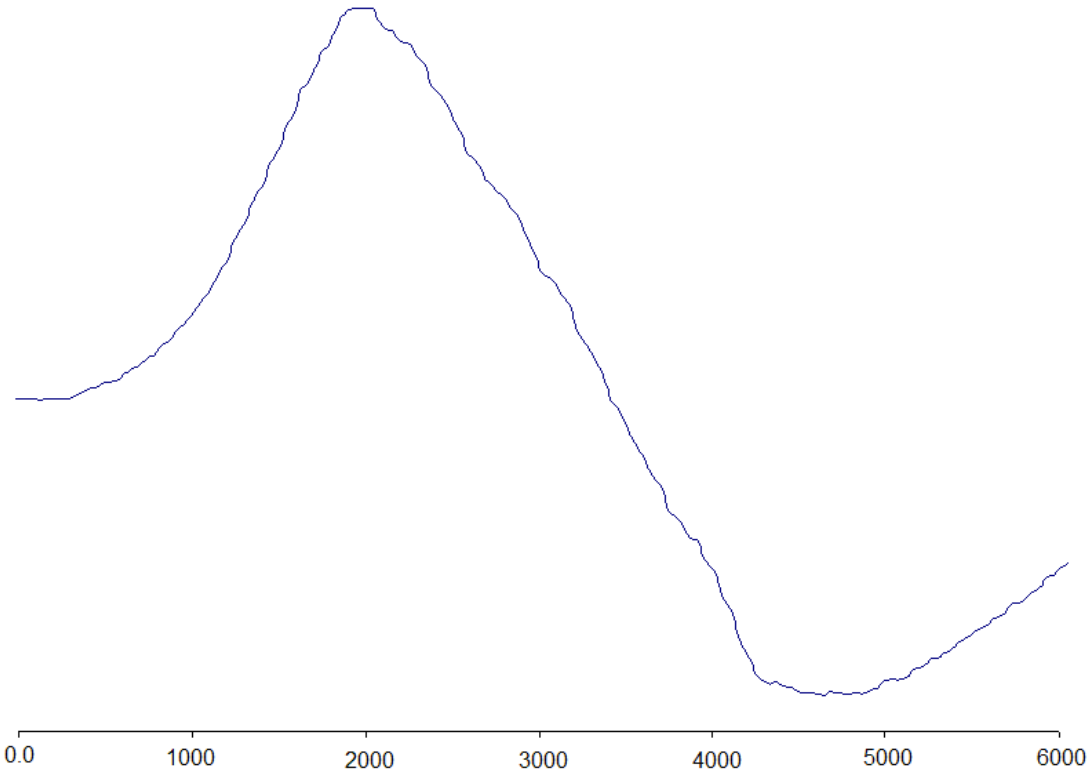

S23: X-band ESR spectrum of triazole – based iron(III) complex 1

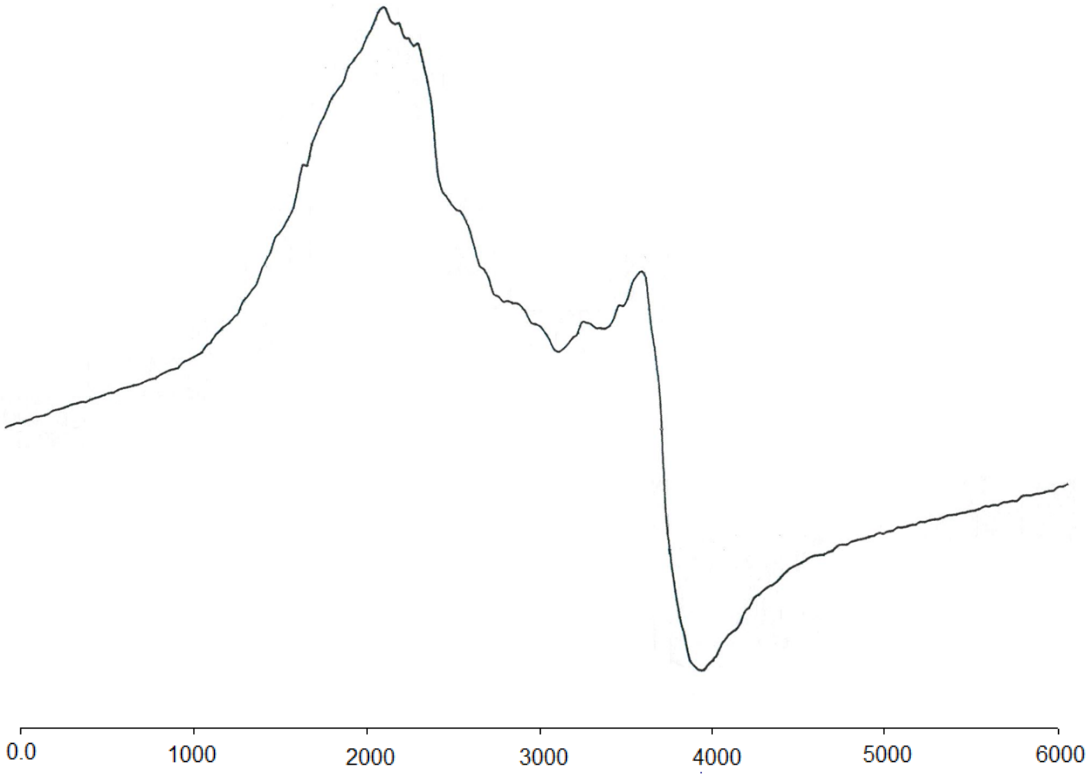

S24: X-band ESR spectrum of triazole – based iron(III) complex 2

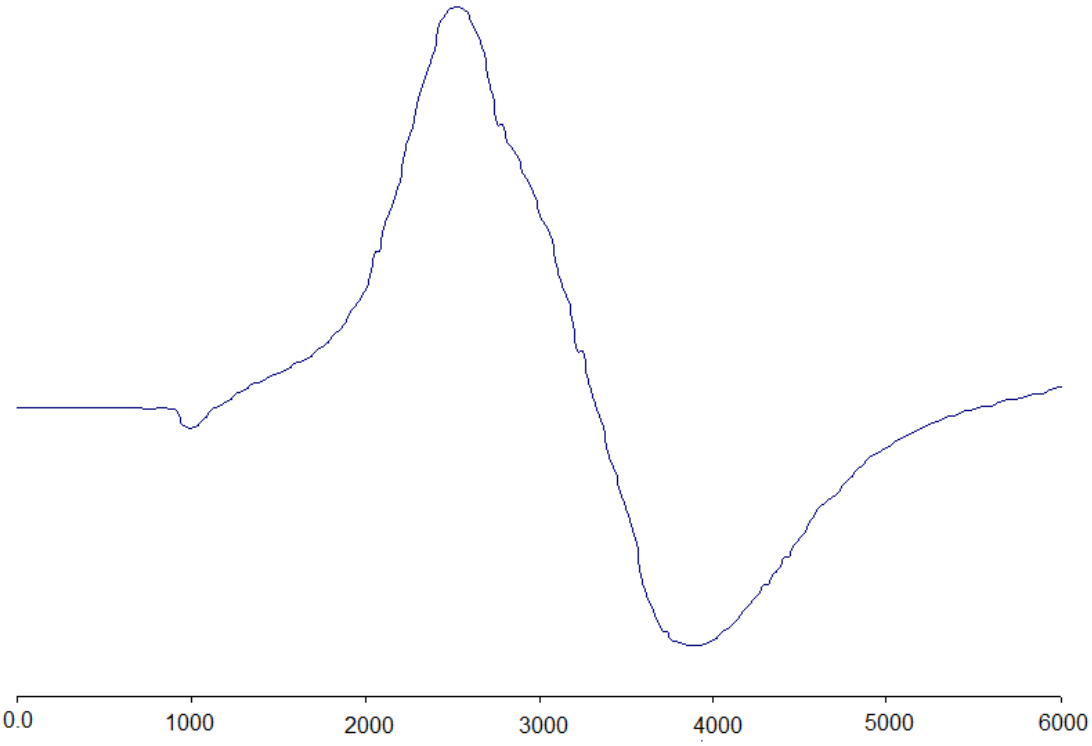

S25: X-band ESR spectrum of triazole – based iron(III) complex 3

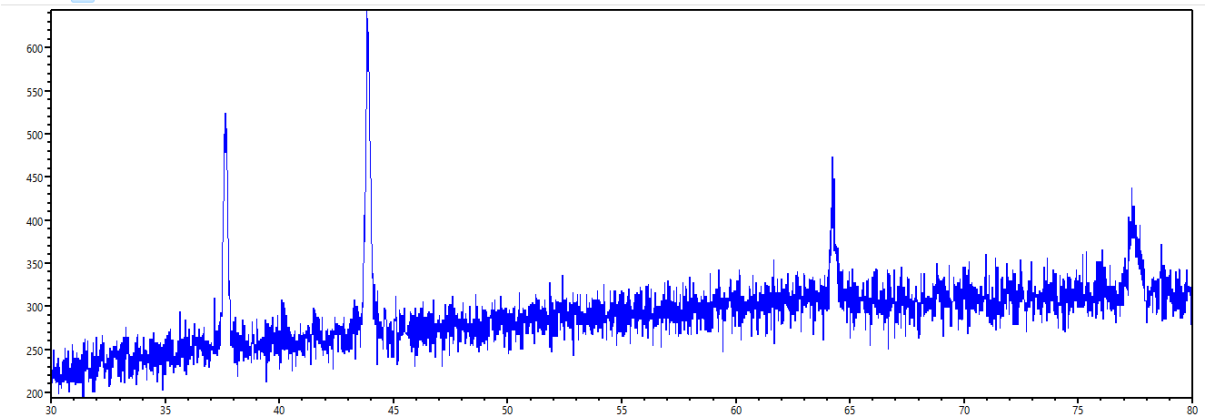

S26: X-ray powder diffraction spectrum of the triazole-based Fe(III) complex **2**

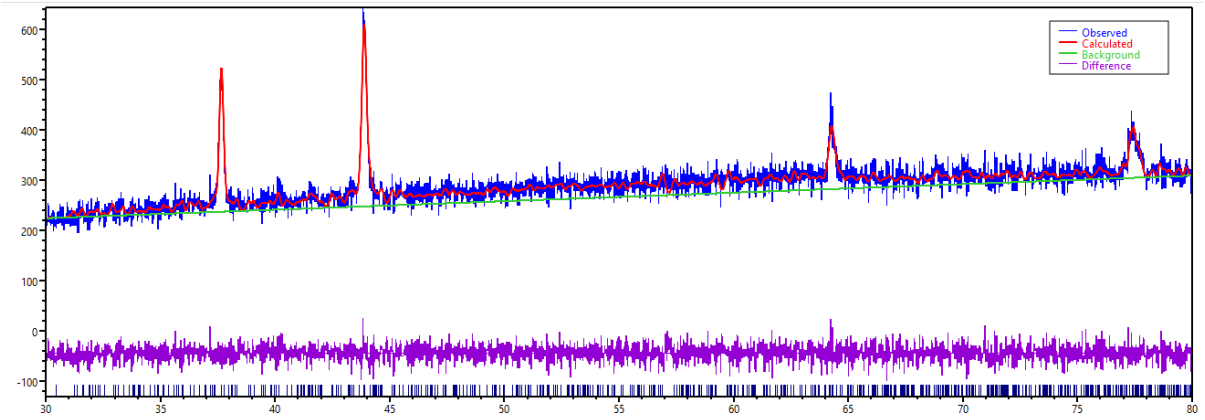

S27: High agreement profile of practical results for powder X-ray diffraction spectrum with theoretical calculations processed by the Rietveld technique in the case of Fe(III) complex **2**

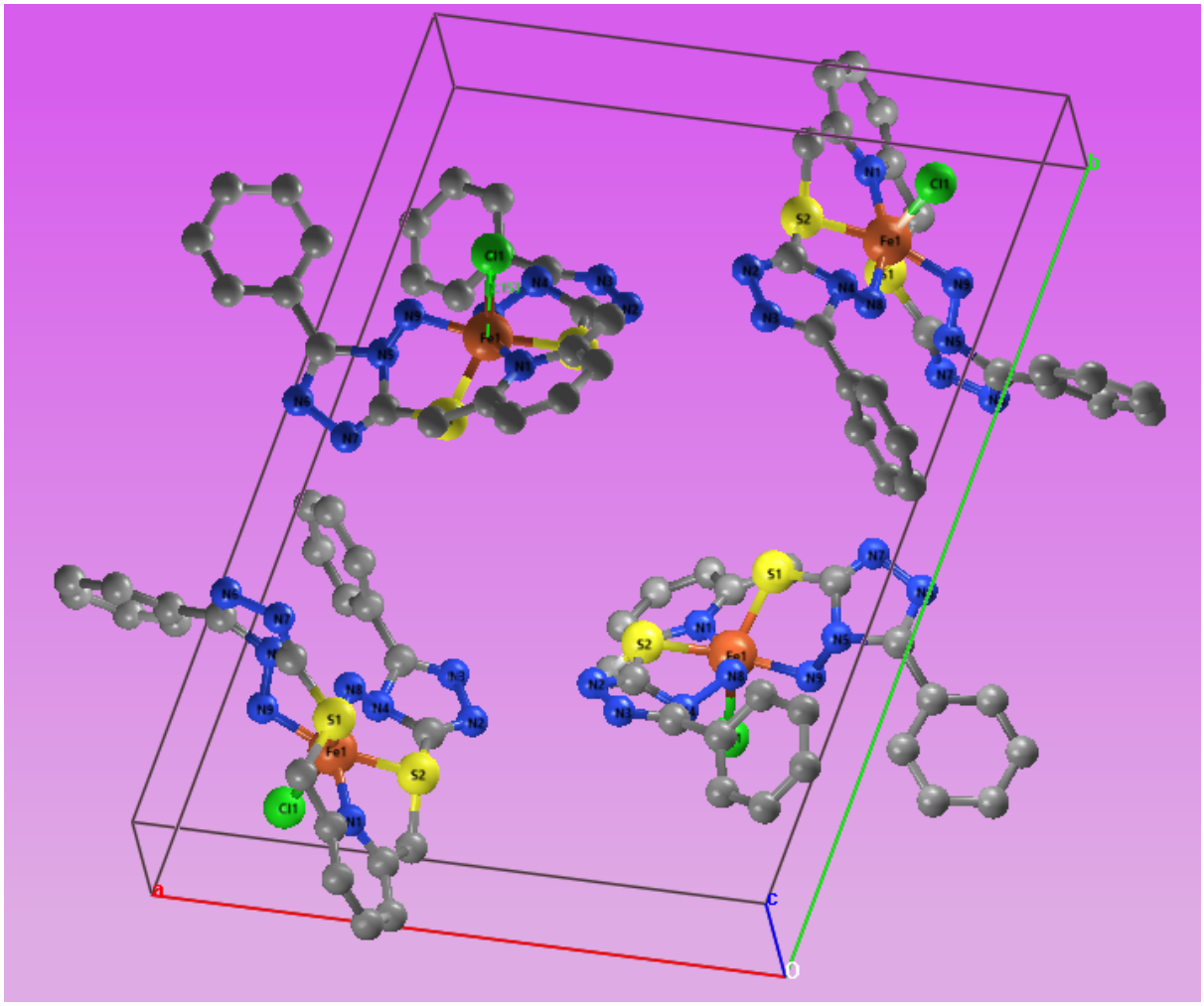

S28: Crystal packing pattern of triazole-based iron(III) comple **2**

S29: Selected bond distances (Å) of triazole-based Fe(III) complex 2

Fe1 center (Θ = 48) τ_6 = 0.8 Octahedral	
Type	**Bond distance (Å)**
N1-Fe1	1.96342
S1-Fe1	2.14846
S2-Fe1	2.14712
N8-Fe1	1.92269
N9-Fe1	1.92091
Cl1-Fe1	2.15345

S30: Selected bond angle (°) of triazole-based Fe(III) complex 2

Fe1 center (Θ = 48) τ_6 = 0.8 Octahedral	
N1-Fe1-S1	77.7
N1-Fe1-S2	75.76
N1-Fe1-N8	155.62
N1-Fe1-N9	126.98
N1-Fe1-Cl1	84.82
S1-Fe1-S2	109.53
S1-Fe1-N8	107.69
S1-Fe1-N9	80.34
S1-Fe1-Cl1	140.83
S2-Fe1-N8	80.09
S2-Fe1-N9	157.2
S2-Fe1-Cl1	99.48
N8-Fe1-N9	77.28
N8-Fe1-Cl1	102.66
N9-Fe1-Cl1	82.86

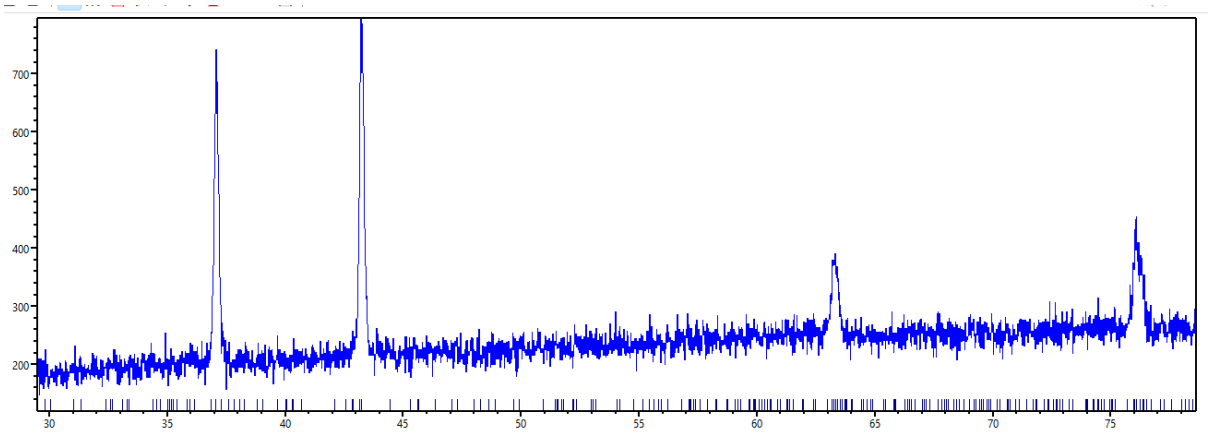

S31: X-ray powder diffraction spectrum of the triazole-based Fe(III) complex **3**

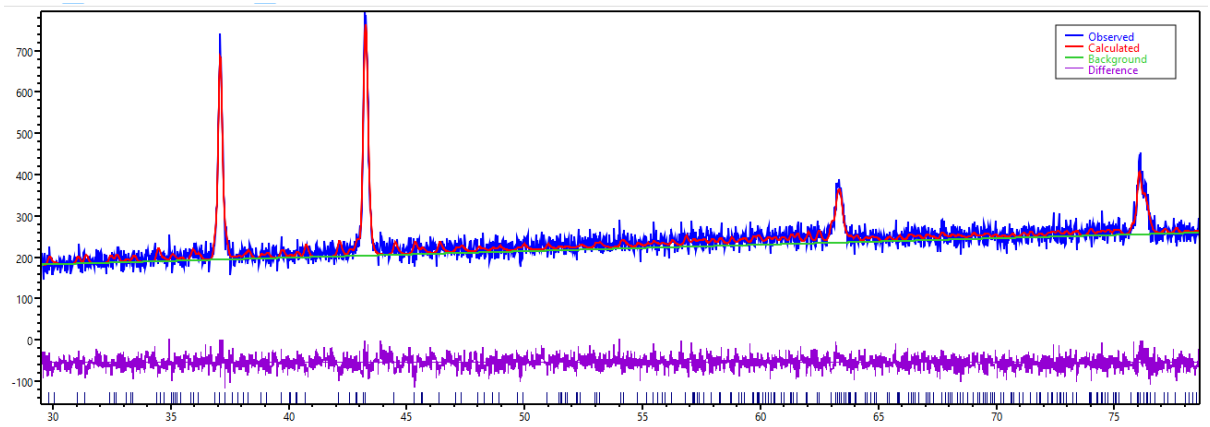

S32: High agreement profile of practical results for powder X-ray diffraction spectrum with theoretical calculations processed by the Rietveld technique in the case of Fe(III) complex **3**

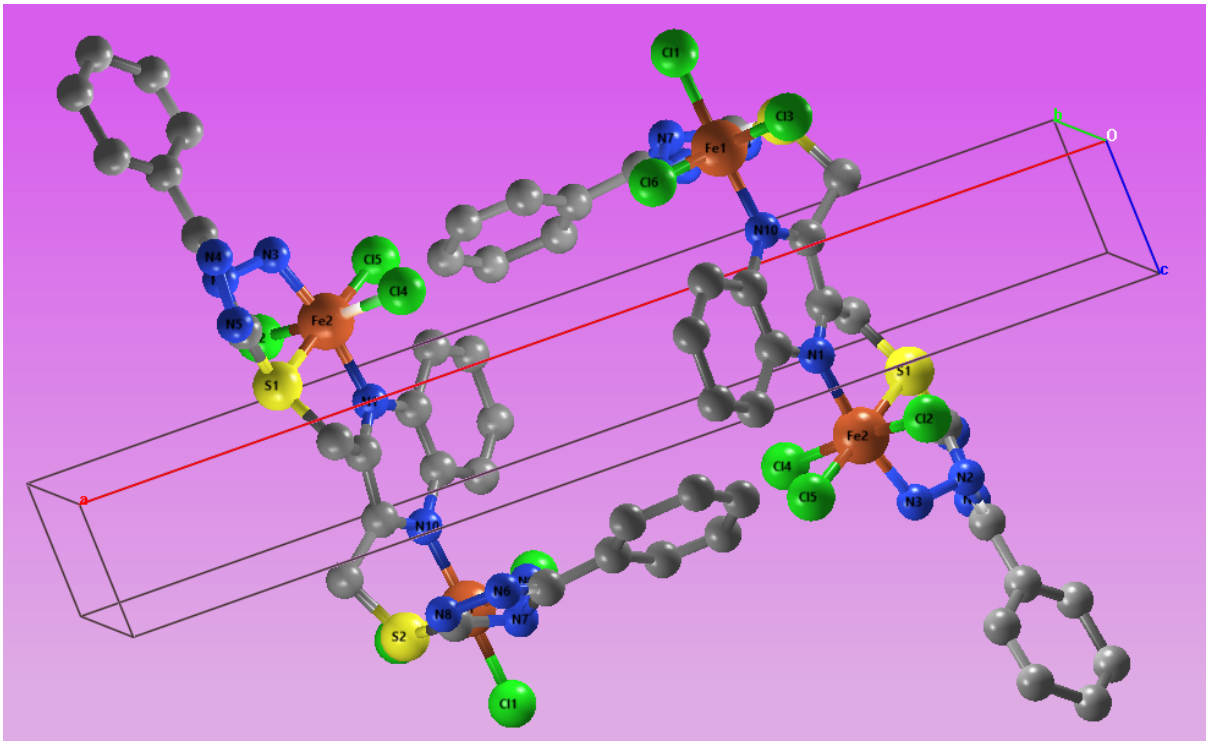

S33: Crystal packing pattern of triazole-based iron(III) comple **3**

S34: Selected bond distances (Å) of triazole-based iron(III) complex 3

Fe1 centre (Θ = 53) τ_6 = 0.88 Octahedral		**Fe2 centre (Θ =51) τ_6 = 0.85 Octahedral**	
Type	**Bond distance (Å)**	**Type**	**Bond distance (Å)**
Fe1…….. Fe2	6.669		
N9-Fe1	1.915	N1-Fe2	1.922
S2-Fe1	2.141	N3-Fe2	1.907
N10-Fe1	1.910	S1-Fe2	2.122
Fe1-Cl1	2.151	Cl2-Fe2	2.147
Fe1-Cl3	2.164	Cl4-Fe1	2.153
Fe1-Cl6	2.153	Cl5-Fe1	2.150

S35: Selected bond angle (°) around Fe1 and Fe2 cores of complex 3

Fe1 centre (Θ = 53) τ_6 = 0.88 Octahedral		**Fe2 centre (Θ =51) τ_6 = 0.85 Octahedral**	
N9-Fe1-S2	85.34	N1-Fe2-N3	165.69
N9-Fe1-N10	89.01	N1-Fe2-S1	80.33
N9-Fe1-Cl1	92.84	N1-Fe2-Cl2	89.45
N9-Fe1-Cl3	178.59	N1-Fe2-Cl4	92.81
N9-Fe1-Cl6	90.4	N1-Fe2-Cl5	97.32
S2-Fe1-N10	83.75	N3-Fe2-S1	85.4
S2-Fe1-Cl1	94.46	N3-Fe2-Cl2	92.8
S2-Fe1-Cl3	93.26	N3-Fe2-Cl4	87.78
S2-Fe1-Cl6	175.08	N3-Fe2-Cl5	96.97
N10-Fe1-Cl1	177.32	S1-Fe2-Cl2	94.77
N10-Fe1-Cl3	90.83	S1-Fe2-Cl4	96.74
N10-Fe1-Cl6	93.73	S1-Fe2-Cl5	177.36
Cl1-Fe1-Cl3	87.28	Cl2-Fe2-Cl4	168.48
Cl1-Fe1-Cl6	88.2	Cl2-Fe2-Cl5	83.98
Cl3-Fe1-Cl6	91.01	Cl4-Fe2-Cl5	84.53

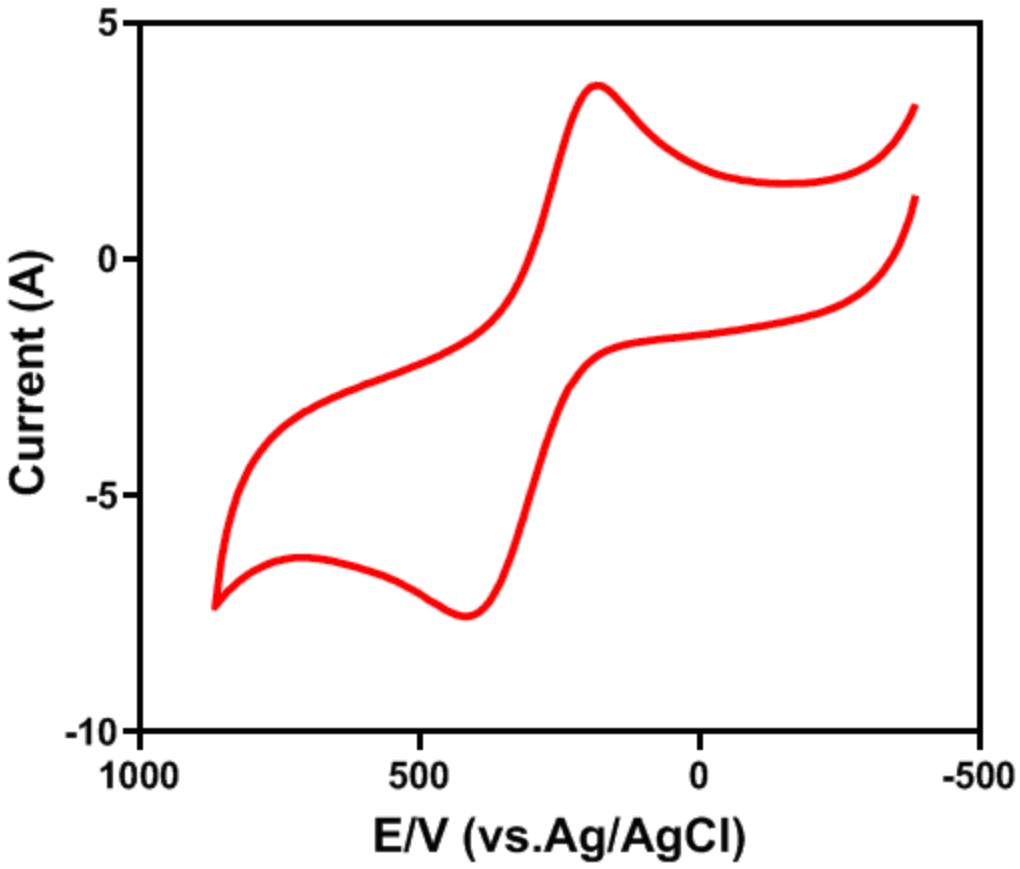

S36: Cyclic voltammogram of triazole – based iron(III) complex 1

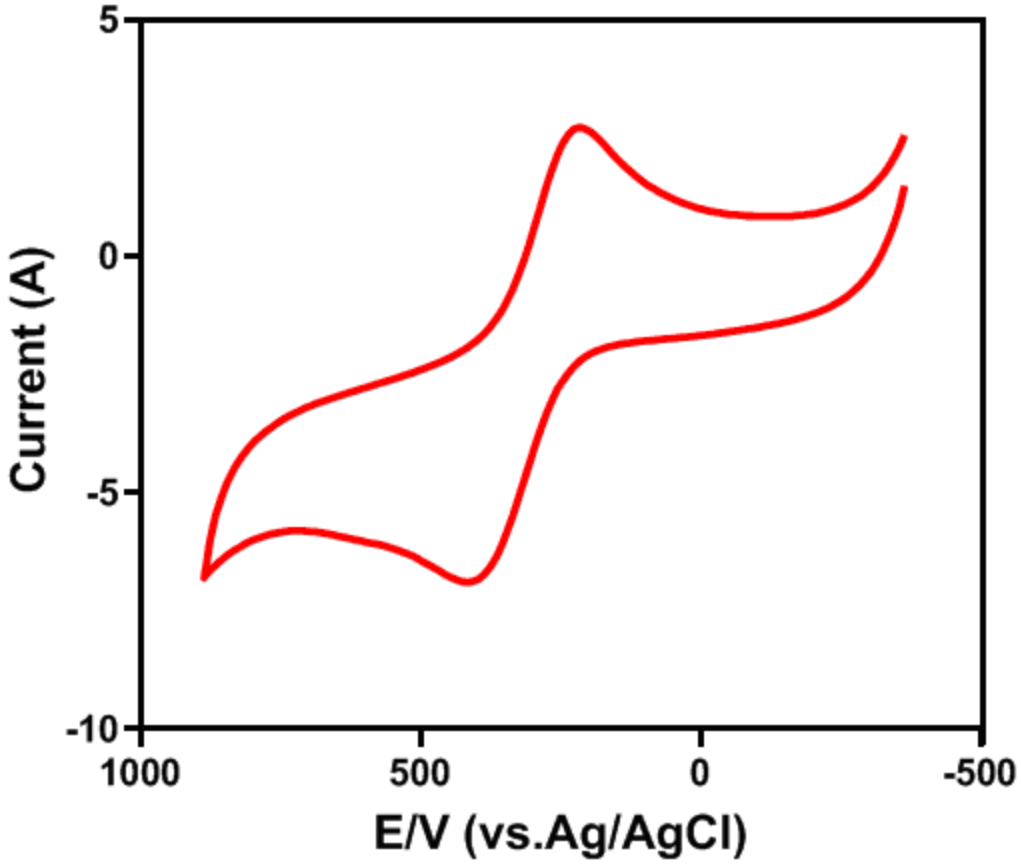

S37: Cyclic voltammogram of triazole – based iron(III) complex 2

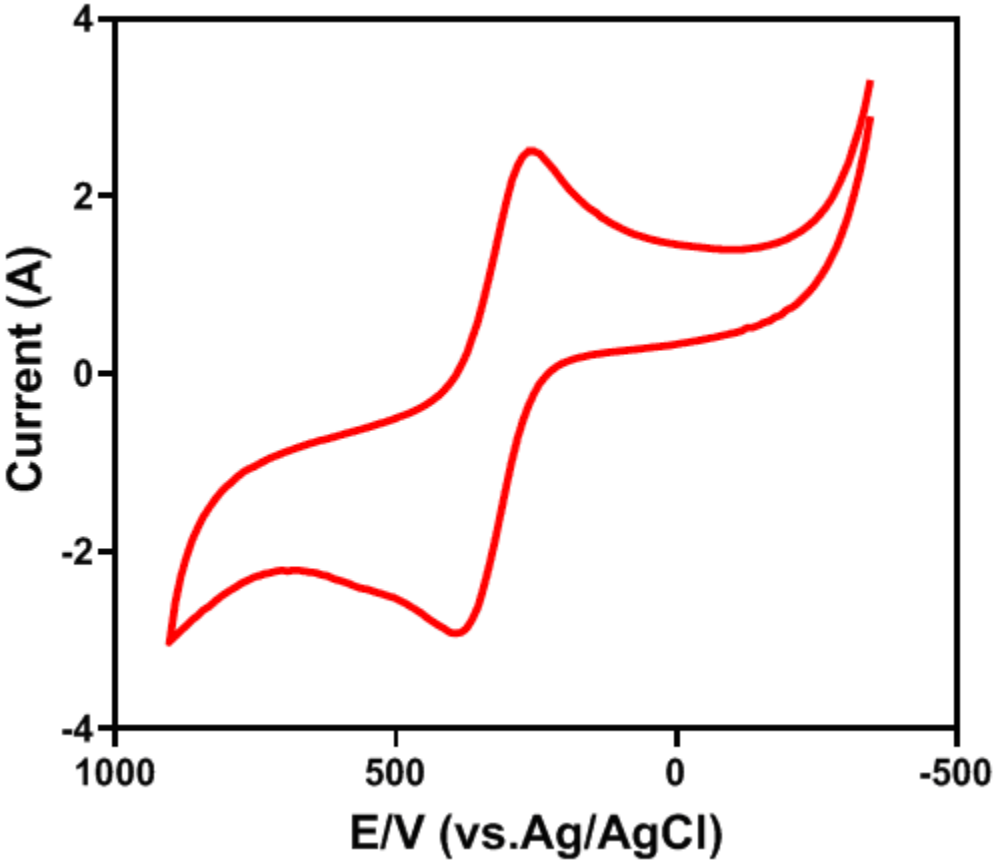

S38: Cyclic voltammogram of triazole – based iron(III) complex 3

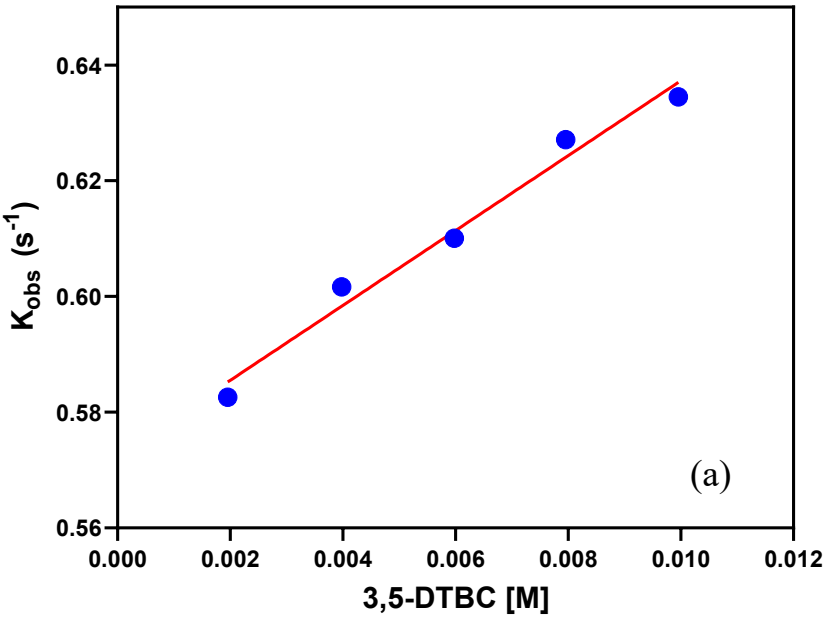

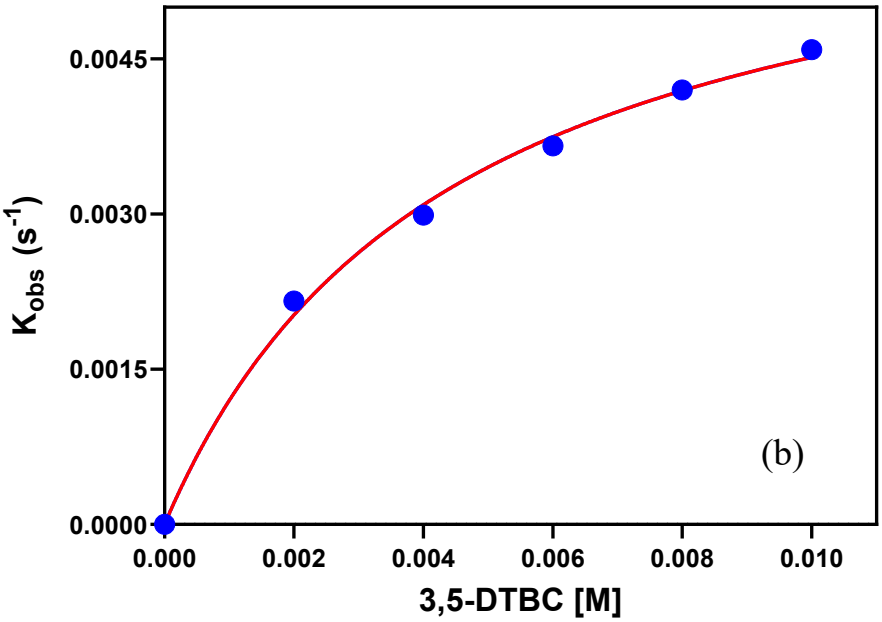

S39: Graphical representation of the initial rate versus 3,5-DTBCH_2 concentration for (a) the fast step and (b) the slow step in case of complex **2**.

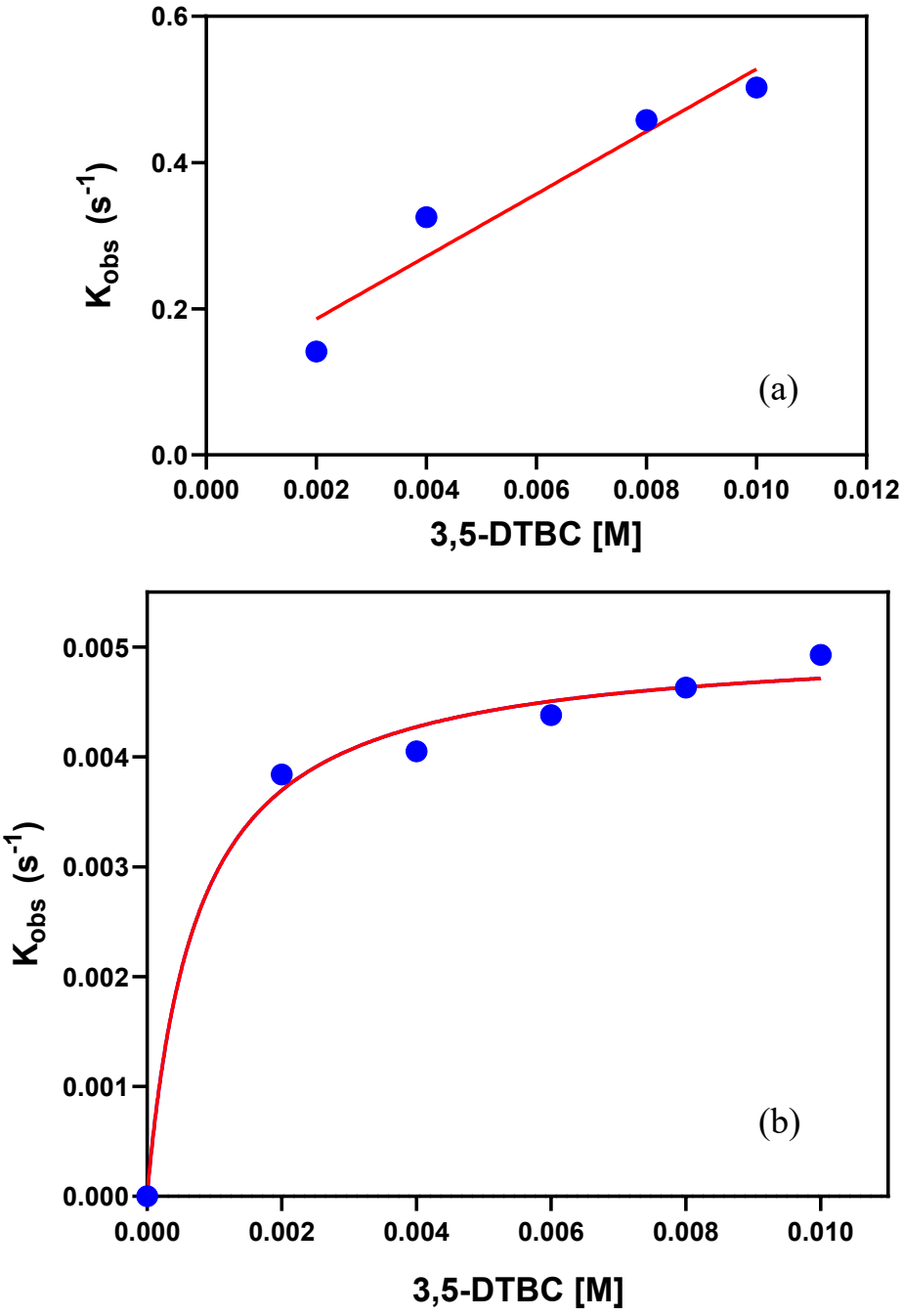

S40: Graphical representation of the initial rate versus 3,5-DTBCH_2 concentration for (a) the fast step and (b) the slow step in case of complex **3**

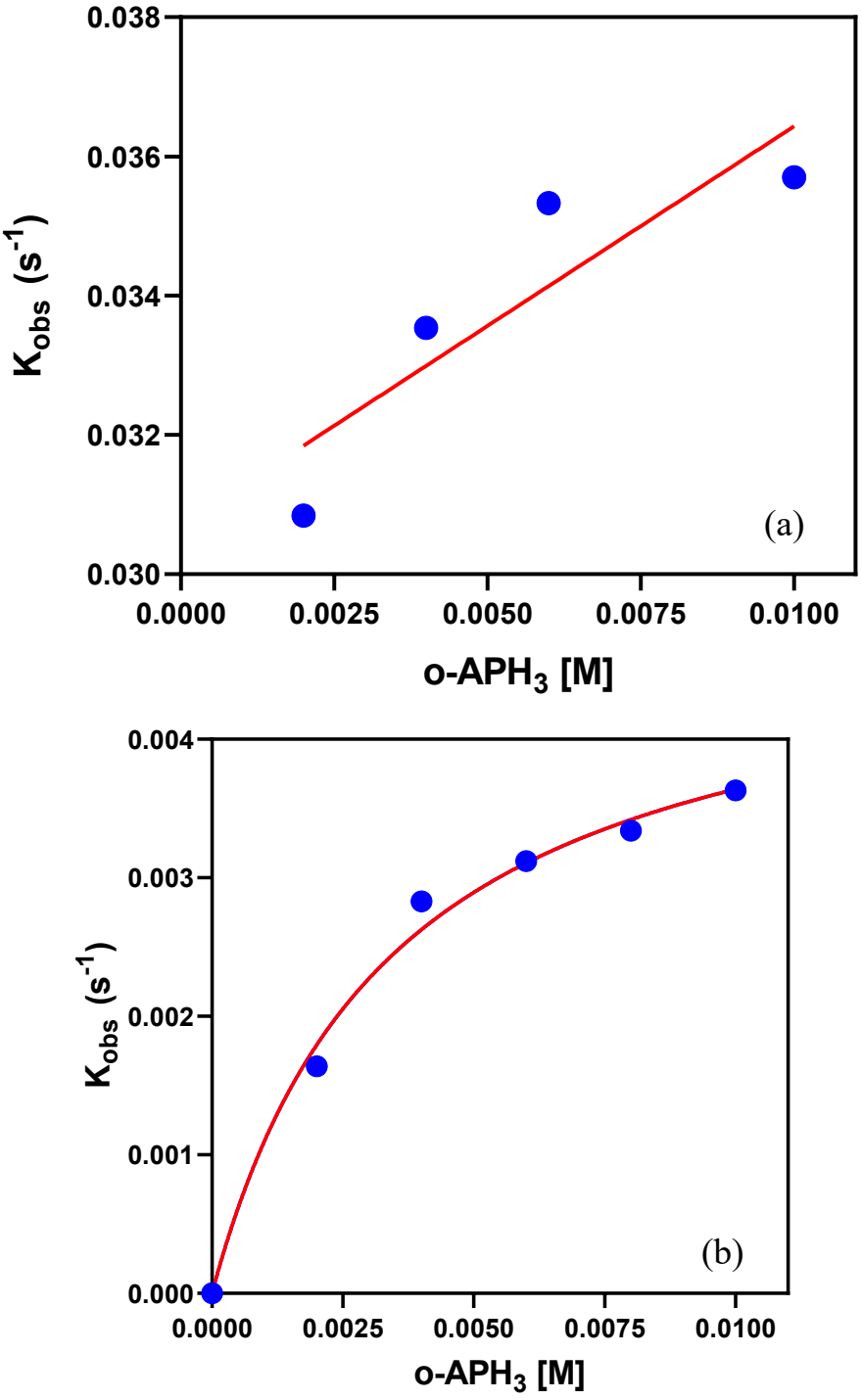

S41: Graph of the initial rate versus concentration of *o*-APH_3 for (a) the fast step and (b) the slow step in the case of complex **2**.

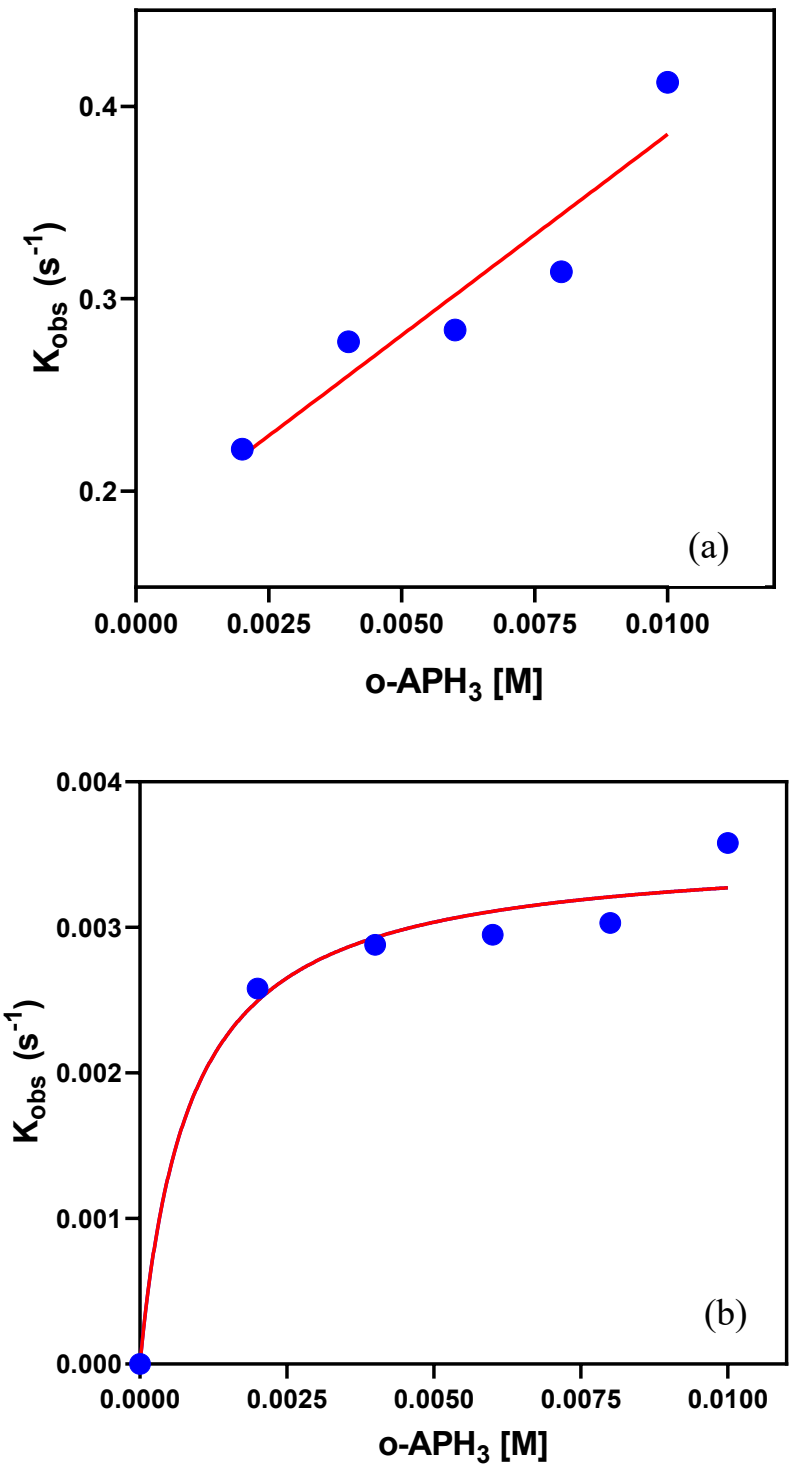

S42: Graph of the initial rate versus concentration of *o*-APH_3 for (a) the fast step and (b) the slow step in the case of complex **3**.